AFIT/MS/ENY/20-255

ALTERNATIVE MATERIAL FOR HIGH-SPEED PROJECTILE CASING

THESIS

Presented to the Faculty

Department of Aeronautics and Astronautics

Graduate School of Engineering and Management

Air Force Institute of Technology

Air University

Air Education and Training Command

in Partial Fulfillment of the Requirements for the

Degree of Aeronautical Engineering

Andrew W. Beard, B.S. in Mechanical Engineering

Capt, USAF

26 March 2020

AFIT/MS/ENY/20-255

ALTERNATIVE MATERIAL FOR HIGH-SPEED PROJECTILE CASING

Andrew W. Beard, B.S. in Mechanical Engineering
Capt, USAF

Committee Membership:

Anthony N. Palazotto, PhD
Chairman

Major Ryan A. Kemnitz, PhD
Member

Meir Pachter, PhD
Member

ADEDJI B. BADIRU, PhD
Dean, Graduate School of Engineering and Management

Abstract

A high-speed projectile impact is a highly complex dynamic problem that can be simplified with the use of finite element analysis solvers. Abaqus/Explicit was used to evaluate the impact of various projectiles using a plane strain setup. Using a baseline stainless steel projectile, the proposed sandwich construction design was analyzed and compared to the baseline projectile. The overall goal was to see if a new composite casing could perform similarly to the simple baseline projectile. The sandwich construction used stainless steel, tungsten, and silicon-carbide reinforce aluminum as outer and inner shell materials. The core material was created using additive manufacturing of inconel 718. The inconel 718 core is a triply periodic minimal surface structure manufactured to provide the projectile casing with high stiffness and strength while reducing material used to manufacture it. A monolithic concrete target using a brittle cracking model for a projectile hitting a concrete wall in order to simulate a projectile impacting a bunker, road, or other concrete structure. Each projectile was evaluated using either the Johnson-Cook damage model or the Hashin damage model depending on if the shell materials were ductile metals or a metal matrix composite. By implementing the sandwich design, the negatives and benefits can be considered for mission feasibility.

Acknowledgements

I would like to thank Dr. Anthony Palazotto for his unwavering support for me as a student. Additionally, I would like to thank the other professors that made this paper possible including Maj Brian Bohan, Dr. Pachter, and Maj Ryan Kemnitz. Lt Col Derek Spear, thank you asking me questions about my research and providing early support for learning Abaqus. Also, thanks to all the friends I have met at AFIT because we never let each other go it alone. None of this would be possible without my parents who raised me and taught me the most important values I know. Last, but far from least, I thank my loving wife and son for dealing with the long days I spent on this research and other AFIT work. I love the both of you so much.

Andrew W. Beard

Table of Contents

Page

List of Figures

List of Tables

List of Abbreviations

Abbreviation		Page
TPMS	Triply Periodic Minimal Surfaces	3
MMC	Metal Matrix Composite	3
AFRL	Air Force Research Laboratory	5
CG	Center of Gravity	5
FEM	Finite Element Method	13
JC	Johnson-Cook	19
SiCAl	Silicon-Carbide Reinforced Aluminum	28

List of Symbols

Symbol		Page
C_u	Compressive Denotation	22
L_u	Longitudinal Shear Denotation	22
P_u	Transverse Shear Denotation	22
$X^{Denotation}$	Strength in Fiber Direction	22
$Y^{Denotation}$	Strength Transverse Direction	22
$S^{Denotation}$	Shear Strength	22
F_f^t	Tensile Damage Initiation of Fiber	22
F_f^c	Compressive Damage Initiation of Fiber	22
F_m^t	Tensile Damage Initiation of Matrix	22
F_m^c	Compressive Damage Initiation of Matrix	22
α	Fiber Tensile Shear Stress Coefficient	22

ALTERNATIVE MATERIAL FOR HIGH-SPEED PROJECTILE CASING

I. Introduction

1.1 History

The oldest account of the use of a war machine is written in the Bible around 800 years B.C. Primitive yet powerful weapons such as the ballista and catapult were able to hurl projectiles too heavy for human power alone to turn into destructive tools. Later inventions like trebuchets were used to siege large structures by slinging the projectiles into the walls–destroying them, and allowing military forces to breach the structure. It was not until around the 13th century that gunpowder was first used to fire a projectile at previously unattainable speeds. Cannons were used well into the 19th century to send iron balls the size of a fist or larger through ship hulls or stone walls with power and accuracy. Although traditional cannons have become obsolete, mortars still use the same premise to launch an explosive charge over a long distance [1]. Mortars were particularly useful during WWII in order to pierce through concrete bunkers set in strategic and hard to reach locations on the battlefield. Today, bunkers, armor, and other structures are designed to be hard to penetrate with ordinary projectiles. The main projectiles used to penetrate these structures today use a long cylindrical projectile that contain explosive material which detonates during the impact. The concept of an exploding projectile is not new, but new materials and methods of manufacturing allow for new projectile solutions and provide better options. The questions posed in this thesis will be based on finding alternative projectiles than today's standard projectile and how to bring it to the

next level–from a ballista to a mortar, or a bowstring to gunpowder.

Bunker busting projectiles have evolved over time as shown in Fig. 1, but the same overall design is present throughout. A cylindrical outer casing holds all the explosives and other components inside and a sharp-pointed warhead is mounted at the tip to allow for added penetration. Other designs have expanded on these features and that was what this research effort sought to do as well. [2]

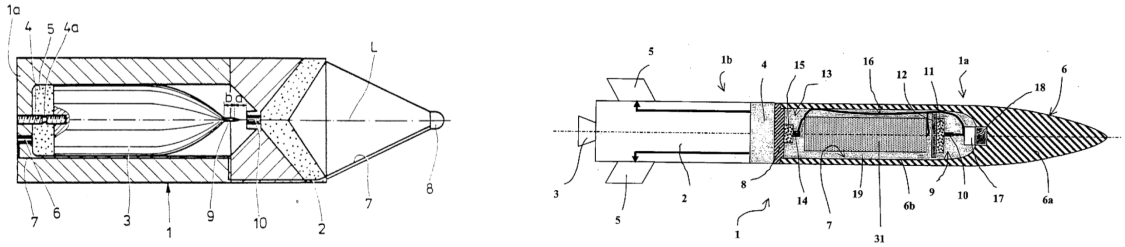

(a) 1943 Warhead Against Fortified or Armored Targets

(b) 2006 Anti-Bunker Munition

Figure 1. Both of the warheads shown have similar intended uses and apply similar aspects of the design such as the internal sliding detonation device. [3] [4]

1.2 Objective

The objective of this research was to create a replacement projectile casing that is lighter, thinner and performs similarly to a standard stainless steel projectile. Previous research has been done using a scaled down version of projectiles currently being used as "bunker busters", and this effort used a similar approach. By changing the casing design, there should be a noticeable change in the energy transferred, penetration depth, and other observations throughout the impact. By using alternative materials for the outer casing, the projectile will perform differently from the solid stainless steel casing projectile. Some aspects of the new design may be favorable or prove to be worse than today's standard.

Since the goal of this paper is to find out whether an alternative casing design can perform as well or better than a solid steel casing projectile, the projectile casing

will be made of a sandwich structure using stainless steel, tungsten, and silico-carbide reinforced aluminum as the outer and inner shell materials. The core of the sandwich will be made of an inconel 718 lattice structure based on triply periodic minimal surfaces, TPMS. On impact, the shell makeup should allow the projectile to bend and twist while remaining intact until the maximum penetration depth of the target has been reached. The projectile variations will be compared by the penetration depth, kinetic energy transfer, damage dealt to the concrete wall, and observations seen within the simulations. It would be ideal if the composite projectile performs similarly to the steel projectile since it will be a potential replacement solution. The failure of each projectile will be analyzed in order to find the primary causes and predict how to solve the problem.

1.3 Project Motivation

Unlike previous work done on projectiles, this research uses projectile casings made of alternate materials such as the TPMS lattice and metal matrix composite materials, MMC, instead of a single material such as solid stainless steel. The performance of a 6.35 mm thick solid stainless steel casing projectile will be compared with various configurations of projectiles that will be outlined in Chapter II. Creating a new design for a projectile could have an impact on weight savings and amount of material used. By reducing the weight of an individual projectile, an aircraft is able to carry more without increasing the weight of the payload. Everything from increased volume of projectiles to fuel savings would be impacted by a change in unit weight. Additive manufacturing of the casing could potentially reduce the material necessary to create the projectile which aids in material cost savings. Although the manufacturing cost of the projectile will be higher than the standard stainless steel projectile, there would have to be a cost analysis to determine how much fuel money will be saved while the

projectiles are manufactured.

1.4 Overall Assumptions

There were various assumptions made that were used in all simulations in order to simplify the problem and how to evaluate it. The first assumption made was to use a plane strain model in order to see the projectile and wall responses in 2D before going forward with a 3D model. Another assumption made was that the projectile does not experience any perturbations during flight, and it reaches the concrete target with the axis of rotation normal to the concrete targets surface. The concrete wall is assumed to be an isotropic block of concrete that is not reinforced with rebar. Furthermore, a brittle concrete method used in Abaqus explicit was used to compare results of the various projectiles modeled in the 2D case. The brittle failure model is not the most ideal model to use in the high-speed projectile situation, but provides useful information when analyzing the effectiveness of the projectiles and made computations easier.

1.5 Overview

For the remainder of the report, Chapter II covers the background of similar work already accomplished and how the theory of the design was used. Chapter III outlines the methodology used to model the projectile in Abaqus. Chapter IV reports the analysis findings of the various designs and how they differ during impact. Chapter V discusses the results found, estimated trends of projectile performance, and how to improve upon this project in the future.

II. Background

2.1 Previous Research

Richards.

Research was accomplished by individuals who have looked at ways to improve the geometry of these projectiles in order perform as well as or better than the standard munition currently in use. The main focus of the past researchers was beneficial for the additive manufacturing route opposing the route of using alternative materials instead of materials commonly found in projectiles. Drawing from the conclusions of research done on projectiles, it is possible to reduce the casing thickness in order to improve the damage done by the explosives within the projectile. It is important to know where this project stems from and look at the work that has already gone into similar projects. Hayden Richards was the first to begin work on creating a warhead that could be additively manufactured instead of the normal material subtraction methods or molding. Richards took a scaled down version of a warhead design received from the Air Force Research Laboratory, AFRL, to use as a starting point with the design. The use of additive manufacturing has been growing rapidly in the last decade and the idea of using it to create munitions was still very foreign. The question Richards set out to answer was: Can additively manufactured munitions be as effective as normally manufactured munitions of the same caliber? Using topology optimization, Richards was able to design a projectile that could be additively manufactured, used less material for the outer casing, and could withstand the impact and penetration necessary to match the abilities of a normal steel projectile as shown in Fig. 2. The topology optimization resulted in a cartridge that is long and cylindrical with a pointed nose, but the inside of the munition contains a lattice-type structure that keeps the center of gravity (CG) forward and also reinforces the nose while providing a

thinner outer casing for added lethality. Once designed and printed, the projectile was tested against a concrete target, shown in Figs.3 and 4, to analyze how it performed. The projectile was manufactured and fired at a concrete target at 450 m/s. The internal lattice structure showed that the projectile could survive the best up to the point where the lattice structure becomes less dense, which was the ultimate location of failure shown in Fig.5. [5] [6]

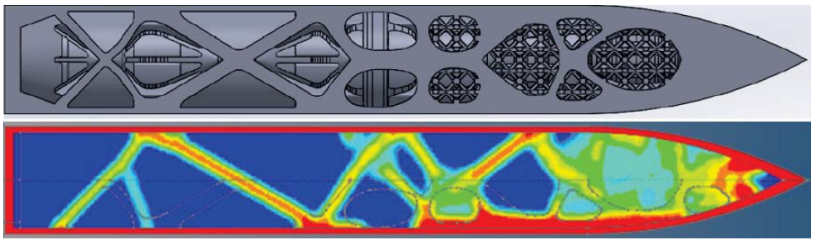

Figure 2. This is the design Richards initially came up with. Note that the inner lattice is dense near the nose of the projectile.

Figure 3. The concrete target Richards used was not reinforced and was contained by a thin cylindrical outer layer of steel.

The main features of Richards' design that were adopted in this paper were the ogive nose shape, the overall size of the projectile, the type of monolithic target used in live fire testing, the additive manufacturing of the projectile, and the idea of making the outer shell of the projectile thinner.

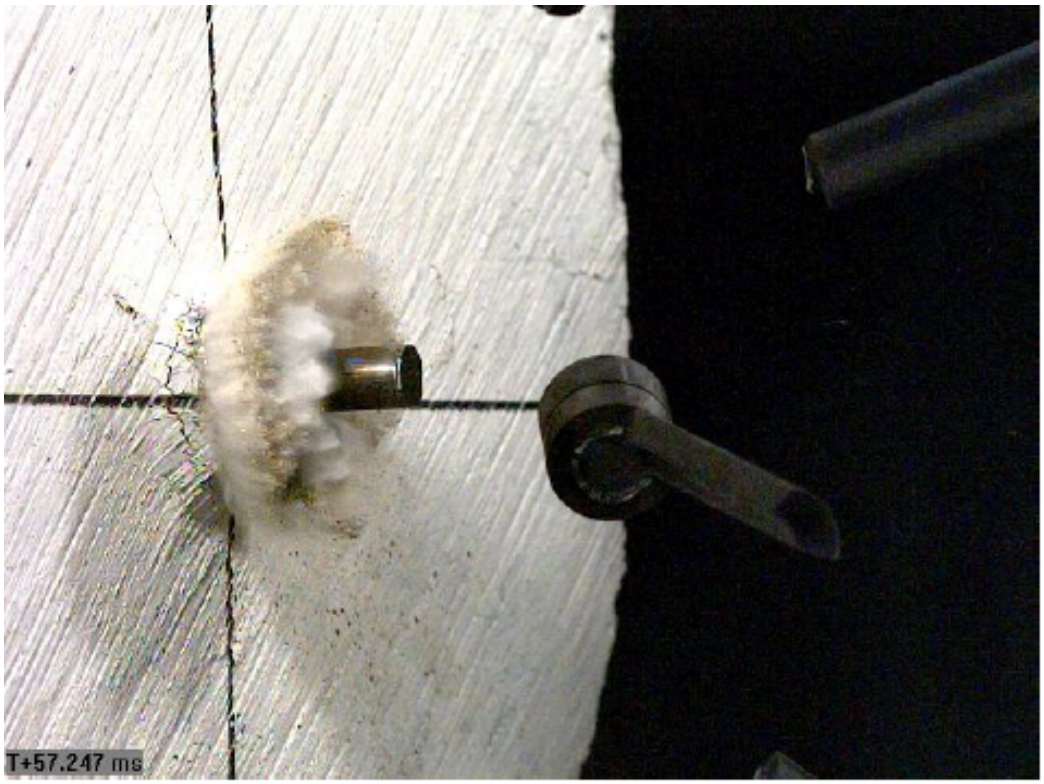

Figure 4. Richards' projectile is shown colliding with the concrete target and shows signs of radial cracking in the concrete. The large metal object close behind the projectile is part of the sabot used to contain the projectile for firing it.

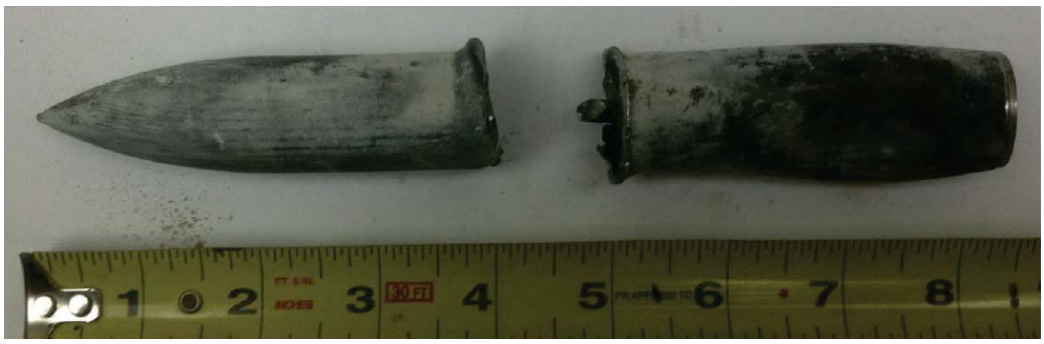

Figure 5. The projectile failed at the midpoint of the shaft after the transition from dense lattice to sparse lattice.

Graves and Provchy.

Graves and Provchy built on Richards' initial design but focused on refining the design and redefining the test with different target types. Graves set out to refine the lattice structure in order to improve the integrity of the projectile to better survive the impact shown in Fig.6. The internal lattice structure needed to be smoothed out in order to prevent a specific point of failure that was seen in Richards' testing. Graves's project heavily relied on topological optimization and also looked at the overall penetration depth similarly to Richards like Fig. 7 shows. Fig. 8 shows that Graves's projectile ended up failing similarly to Richards' projectile as well, so Provchy was the next to improve upon the warhead design. Provchy once again refined the design shown in Fig. 9, but tested the projectile against three consecutive targets and in order to succeed the projectile had to damage each of the three targets. This was different because both Graves and Richards were using a semi-infinite concrete target and analyzing depth of penetration. Provchy also improved upon the Johnson-Cook parameters that Graves used to more accurately represent what the failure would look like. [7] [8]

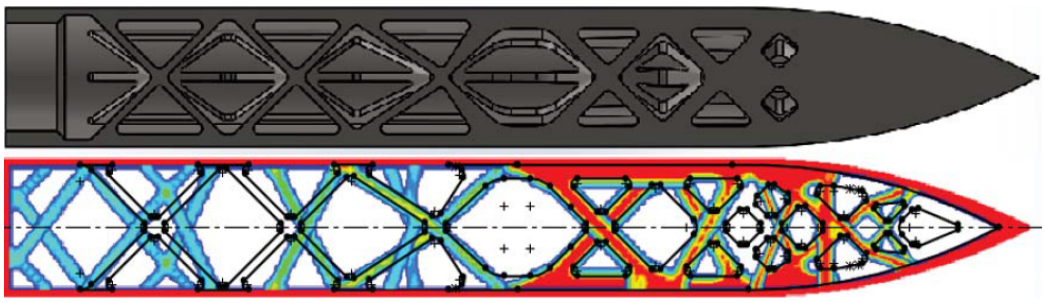

Figure 6. Graves' improved projectile design.

Figure 7. Graves' projectile is shown embedded within the concrete target. Note that the projectile is relatively intact.

Figure 8. Graves' projectile failed similarly to Richards'.

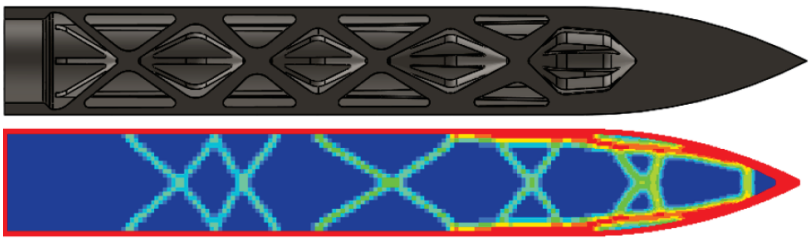

Figure 9. Provchy's design.

The various aspects adopted from these research efforts were the material properties for additively manufactured metals and the target used by Graves which was similar to Richards' target.

Patel.

The most recent research has been conducted by Aadit Patel [5] who took the existing design but used a steel shell with an aluminum lattice on the inside of the projectile as shown in Figs. 10 and 11. The combination of these two metals changed the analysis from a homogenous material (excluding the explosives) to an overall composite material performance as he outlines in his thesis. Patel also incorporated different failure methods such as Johnson-Cook to analyze the projectile and Johnson-Holmquist to analyze the target response at impact. Another key difference was Patel changed the target orientation by positioning three angled targets in the simulation models and the live fire test shown by Fig.12. Patel ultimately found that some of the changes he made from the previous designs negatively impacted the results of his design since the projectile fails catastrophically as in Fig.13. For instance, the nose geometry previously used was solid, but Patel decreased the thickness within the nose and saw catastrophic failure beginning within the nose of the projectile opposed to the mid-section failures experienced in the previous designs. This thickness of the nose allows the projectile to withstand the initial impact against the concrete target,

and also allows for more momentum as it penetrates through the first target and continues to the second and third. [5] [9]

Using Patel's findings, it was clear that the internal aluminum lattice would be of value for the final design in this paper. However, Patel found that the nose used in his design failed to withstand the forces upon impact. Therefore, an internal aluminum lattice would likely be necessary, but the final design should use an ogive shaped nose that contains a denser and stronger material than the additively manufactured aluminum.

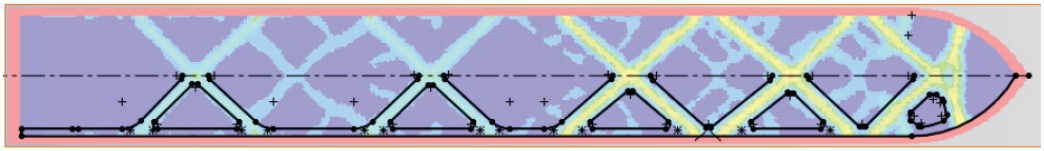

(a) 2-D geometry sketch of aluminum insert.

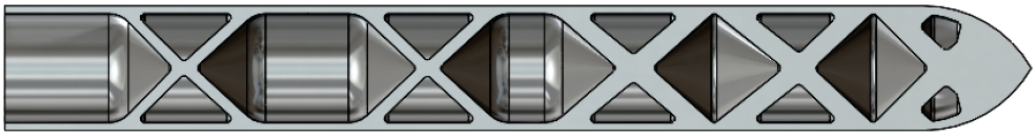

Figure 10. Patel used an aluminum insert to provide extra support for the projectile's impact.

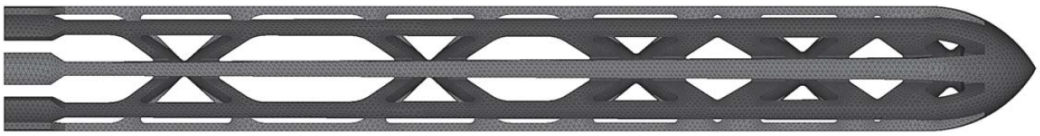

Figure 11. The insert Patel created was additively manufactured.

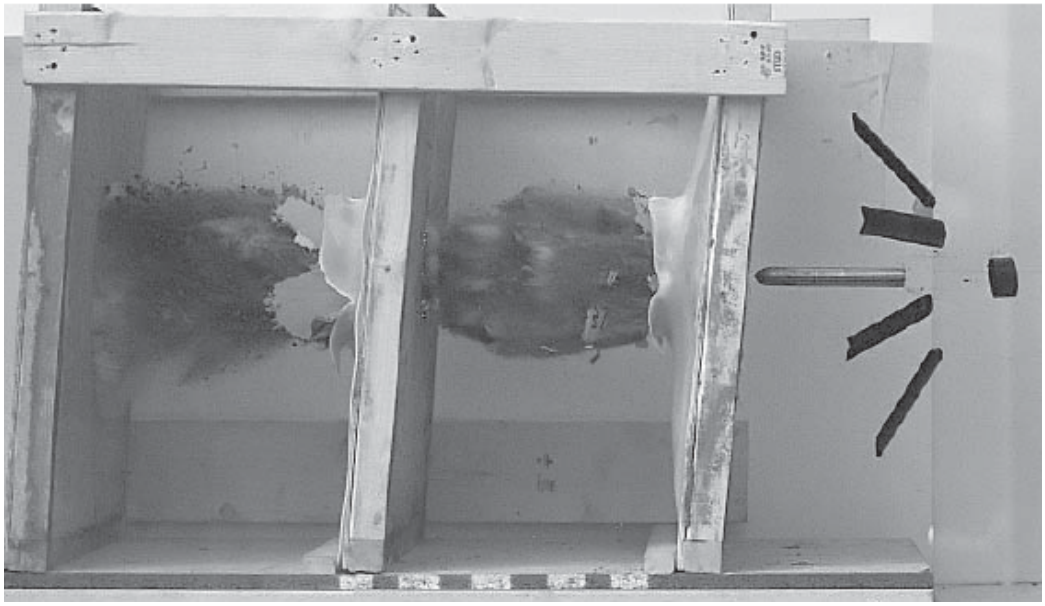

Figure 12. The projectile is shown as a time-lapse going through the targets.

Figure 13. Patel's Projectile catastrophically failed by having the nose splintering on impact with the targets. The insert can be seen surviving at the midpoint of the projectile.

2.2 Theory

Finite Element Method.

This research delves deep into the finite element method, FEM, and how it is used to analyze the responses of both the projectile and target. FEM allows a problem to be discretized into smaller regions called elements where each element has its own properties and interactions with the other surrounding elements. One of the simplest ways to understand what FEM is accomplishing is by using Hooke's law for elasticity. For example, look at a simple one-dimension spring problem where the spring is fixed at one node and a force is acting at the other node as shown in Fig. 14. The displacement of the node with the force acting on it can be found through equilibrium of the system. Once the displacement is solved for, then other solutions can be carried out such as element strain, stress, and more. To elaborate, the specific problem set up in this research has the projectile and concrete target divided into small elements. The projectile is given a velocity of 300 m/s and the wall has set boundary conditions that prevent it from moving freely. When the projectile impacts the concrete wall, the elements are programmed to respond to the collision which sends the response throughout the neighboring elements accordingly. This allows the user to see the stress, strain, energy, and damage response within the projectile and wall. [10]

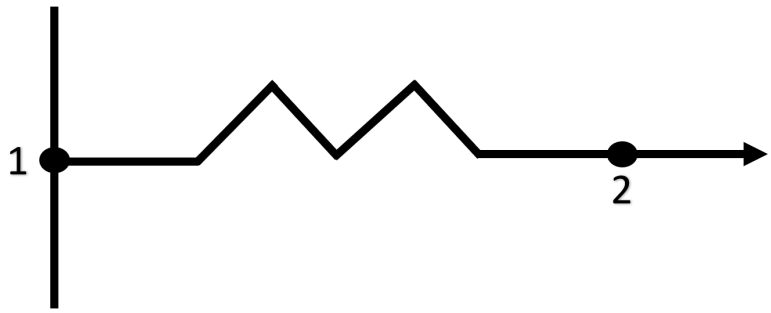

Figure 14. FEA Spring

This particular model uses Abaqus/Explicit in order to predict the outcomes of the model based on what the user wants to find using force balance. There are two types of time dependent methods that can be used to solve FEM problems: Explicit and Implicit. Both methods use algorithms to solve the problem step-by-step, but the explicit model takes a solution at a time step, $t{=}t_i$, and solves the problem for the following time step, t_{i+1}. Step-by-step the problem is solved for each time step in the given time range. [11] [12]

Contact becomes a concern in such complicated dynamic problems that involve impact. For general FEM, Eq. 1 is used as the primary nonlinear differential equation solved according to a balance of force at individual nodes for a given time step, t. By using the external forces (F^{ext}), mass matrix (M), and solution vector (d) at a given time step, the internal forces (F^{int}) can be solved for. F^{int} is a function of the constitutive relationship between stress and strain that is determined by the shape function of the elements used within the model. The process of solving explicitly takes a B-matrix that relates the displacement degrees of freedom to a strain component. By taking the transpose of the B-matrix and using the constitutive relationship between the stress and strain, F^{int} can be solved for by integrating over the volume. Each time step follows the progression of a wave generated by the initial impact. The analyses generates a time relationship characterized by node velocity, acceleration, and thus force represented by Newton's second law of motion.

This process repeats throughout the body for each element and at every time step of interest. This is used by Abaqus/Explicit to calculate the forces acting within the body of the problem which leads to solving for many other cases. However, when contact between multiple bodies occurs, the equation picks up an added term of the contact force vector (F^c) shown in Eq. 2. F^c depends on the contact stiffness calculated between the surfaces of interest which in turn affects Eq.2 by adding a

layer of complexity. Instead of just solving for the interaction between external and internal forces of a body, the contact force vectors contribute to forces experienced by the boundaries of each surface of interest. [13] A "hard" contact using the penalty method was used for the model which allows for instantaneous effects to take place in regards to contact. To expand on the instantaneous aspect, the surfaces of the projectile and concrete will interact when contact is made, but the reactions occur in an instant opposed to gradually. Because of the instantaneous nature of the impact, the projectile transfers all energy into the stress wave and travels through both the projectile and concrete target.

$$F^{ext} = M\ddot{d}(t) + F^{int}(d(t)) \tag{1}$$

$$F^{ext} = M\ddot{d}(t) + F^{int}(d(t)) + F^{c}(d(t)) \tag{2}$$

Abaqus allows for a problem this complex to be solved with relative ease. Since Abaqus has a sophisticated contact algorithm that follows the basics covered above, the program is desirable for the projectile impact problem. Other programs were not considered for this research and it is mainly due to the contact algorithm.

Cracking Model for Concrete.

Various material damage models were used in evaluating the problems because using a purely elastic model for the projectile would be inaccurate and a damaged wall is one of the primary ways to gauge the effectiveness of the projectiles. By using damage criteria for each of the materials used, the models can use the criteria to allow the elements to fail and no longer contribute to the solution to the model. The first of the material models used was the brittle cracking model for concrete.

In order to model the concrete in a way that is accurate, Abaqus has a built in feature to model concrete using a brittle cracking model. This model follows fracture mechanics by using a given displacement of nodes to represent when an element fails and is deleted from the model. As outlined by Table 1, there is a stress v. strain relationship for the concrete elements is shown in Fig. 16 that define when cracking starts to occur known as the tension stiffening curve. When the peak stress is experienced by a given element as shown in Fig.15, the crack starts to form and move until the failure strain is reached allowing the element to be deleted from the model. [14] The models in this research use brittle failure criteria to remove the failed elements from the model. This represents the pulverization of the concrete when it is struck by the projectile and can be represented by dust or debris commonly seen during a high velocity impact. Although using this criteria takes away some accuracy of the model since the concrete matter should not disappear from existence, it is able to represent a loss in concrete volume during impact and is also capable of revealing cracks formed at the impact site or through the stress wave moving through the concrete. The deletion of elements is where this model loses some level of confidence, but for the purpose of this analysis it is used to compare the results of the various projectile types. [15] [16]

Table 1. Concrete Brittle Cracking Criteria

Concrete	
E (Mpa)	20800
v	0.175
Density (kg/mmˆ3)	2.57E-05
Brittle Cracking Tension Stiffening Curve	
Mpa	Strain
2.9	0
1.94393	0.0001
1.30305	0.0002
0.873463	0.0003
0.5855	0.0004
0.392472	0.0005
0.263082	0.0006
0.176349	0.0007
0.11821	0.0008
0.0792388	0.0009
0.0531154	0.001
Brittle Shear Curve	
Mpa	Strain
1	0
0.5	0.0001
0.25	0.0002
0.125	0.0003

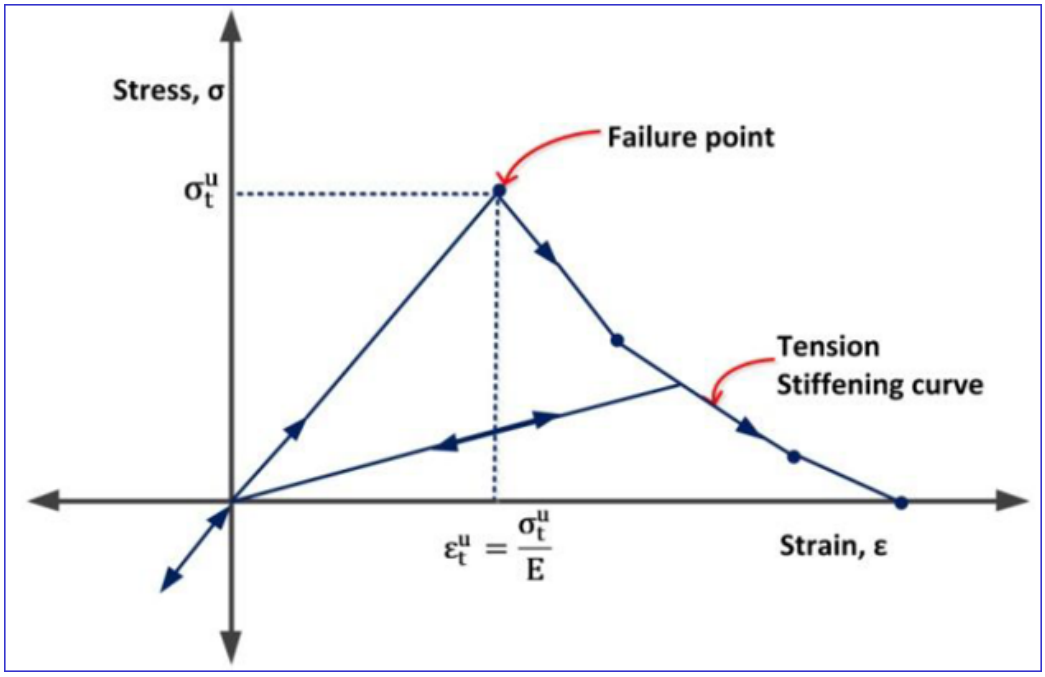

Figure 15. Post-Failure Tension Stiffening Curve of Concrete Elements

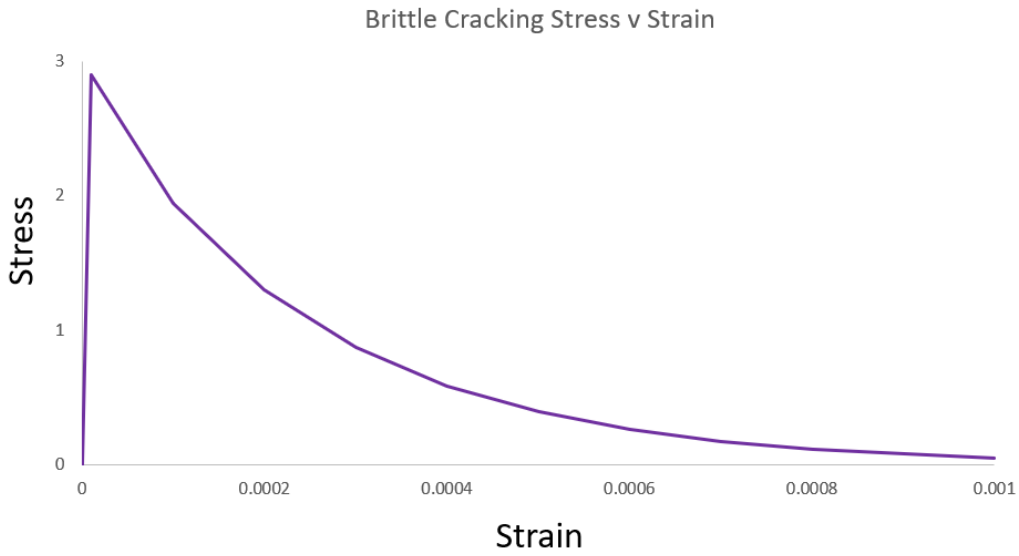

Figure 16. Concrete Stress v. Strain Tension Stiffening Curve

It is important to note that the plastic damage model is also another type of material model that is built into Abaqus and is another way to model concrete. The use of the plastic model was explored, but the feasibility of using it was abandoned because convergence was difficult to achieve for every model. The methodology of the models will be discussed in the next chapter, but the models depend on having the same fixed variables which simply could not occur with the plastic damage model.

The mechanics of projectile penetration have common signs that can be found in accurate models. One is the cone-shaped macro-crack that is formed incrementally as the stress wave propagates through the target. [17] For the 2D plane strain case, the cone can be shown as cracks emanating from the point of contact between the projectile and the concrete target since it is a brittle material. Phenomena that is expected is to see fragmentation of the concrete in a cone-like shape, fractures formed by the stress wave that appear farther into the concrete, and radial fractures originating at the center of impact. [18] While the first two phenomena can be seen in a 2D model, the radial fractures may only appear in a 3D model. [19] [20] [21] [22] [23] [24]

Johnson-Cook Damage Model.

The Johnson-Cook (JC) model is used to characterize the viscoplasticity and damage of ductile materials. For the simulations ran in Abaqus, JC parameters were put into the material properties for each of the ductile materials in the projectile. Stainless steel, aluminum, and tungsten used the JC data so the model could predict how the materials react upon impact. Because of the high strain rates associated with the high-speed projectile impact, a flow stress (σ) must be provided and traced throughout the impact. Eq. 3 shows that the JC equation calculates stress as a function of strain rate ($\dot{\epsilon}$) and homologous temperature (T^*). There is also mean stress(σ_m) and equivalent stress (σ_{eq}) whose ratio is the triaxality of the equation.

The five D's are various constants based on empirical testing for the given material. Those constants: A being the yield stress, B the strain hardening constant, C the strengthening coefficient of strain rate, m the thermal softening coefficient, and n the strain hardening coefficient are used to calculate the stress within the JC equation. Furthermore, the damage equation utilized by the JC equations is shown by Eq.4. As the plastic strain increases, the elements may eventually experience the fracture strain (ϵ_f). This equation uses the mean stress (σ_m), equivalent stress (σ_{eq}), and various damage model constants (D) specific to the material that have been determined by empirical testing in order to check for element failure. Once the strain calculated by Eq.4 equals ϵ_f, the element fails and no longer contributes to the model. The curve at failure decreases to the set ϵ_f called damage evolution. [25] [26]

$$\sigma = (A + Be^n)(1 + Cln\dot{\epsilon}^*)(1 - T^{*m}) \tag{3}$$

$$e_f = [D_1 + D_2 exp(D_3(\frac{\sigma_m}{\sigma_{eq}}))][1 + D_4 ln(\dot{\epsilon}_p^*)][1 + D_5 T^*] \tag{4}$$

Hashin Composite Failure Model.

While JC is used for the ductile materials, Hashin is used for the composites studied in this report. When studying the response of the fibers within the matrix material when compressed in the longitudinal direction, the fibers can fail in a number of ways. Bending, kinking, and fracturing can occur depending on the type of fiber used. For the purpose of this report, the Silicon-Carbide fibers are presumed to be longitudinal within the aluminum matrix. The Hashin and Rotem failure theory states failure can be divided into separate fiber failure and interfiber failure. This failure method requires six parameters in order to predict how the composite will fail: Longitudinal

Table 2. Ductile materials used for projectile parts.

	4340 Stainless Steel	Tungsten (7% Nickel)	Aluminum
E (Mpa)	2.12E+05	3.55E+05	7.10E+04
ν	0.29	0.283	0.33
ρ ($\frac{kg}{m^3}$)	7.85E+03	1.69E+04	2.76E+03
T_m (K)	1.71E+03	3.70E+03	774
A (Mpa)	1.48E+03	1.50E+03	3.24E+02
B (Mpa)	1.84E+03	1.77E+02	1.14E+02
C	.017	.016	.16
$\dot{\epsilon}$	1	1	1
n	0.837	0.12	1.5
m	0.63	1	0.018
$D1$	-0.8	0	0.14
$D2$	2.1	0.56	0.14
$D3$	-0.5	1.5	1.5
$D4$	0.002	0	0.018
$D5$	0.61	0	0

and Transverse Tensile Strength, Longitudinal and Transverse Compressive Strength, and Longitudinal and Transverse Shear Strength. [27] [28] [29]

During each time increment, the stress tensor values for the elements are changed and are put into Eqs.5-8. The equations check for any failures within the composite material-for either the fiber or matrix material.

Table 3. Silicon-Carbide Reinforced Aluminum properties based on Hashin criterion.

E (Mpa)	204000
ν	0.27
ρ ($\frac{kg}{m^3}$)	2.85E+03
Longitudinal Tensile Strength (MPa)	1462
Longitudinal Compressive Strength (MPa)	2990
Transverse Tensile Strength (MPa)	86
Transverse Compressive Strength (MPa)	285
Longitudinal Shear Strength (MPa)	113
Transverse Shear Strength (MPa)	15

$$F_f^t = (\frac{\sigma_{11}}{X^{T_u}})^2 + \alpha\ (\frac{\tau_{12}}{S^L})^2 \tag{5}$$

$$F_f^c = (\frac{\sigma_{11}}{X^{C_u}})^2 \tag{6}$$

$$F_m^t = (\frac{\sigma_{22}}{Y^{T_u}})^2 + (\frac{\tau_{12}}{S^L})^2 \tag{7}$$

$$F_m^c = (\frac{\sigma_{22}}{2S^{T_u}})^2 + [(\frac{Y^{C_u}}{2S^{T_u}})^2 - 1]\frac{\sigma_{22}}{Y^{C_u}} + (\frac{\tau_{12}}{S^L})^2 \tag{8}$$

Where σ_{11},σ_{22}, and τ_{12} are parts of the stress tensor calculated within the model. T_u C_u L_u, and P_u denote tensile, compressive, longitudinal shear, and transverse shear strength respectively.$X^{Denotation}$, $Y^{Denotation}$, and $S^{Denotation}$ denote the strength in the fiber, transverse or transverse direction respectively. F_f^t, F_f^c, F_m^t, and F_m^c are all damage initiation criteria for the fiber in tension, fiber in compression, matrix in tension, and matrix in compression respectively. Finally, α is the fiber tensile shear stress coefficient that is used for the tensile equations.

Inconel TPMS Failure Criteria.

At the time of this research there is no damage criteria for inconel 718 in a primitive TPMS structure. In replacement of such criteria, the ultimate strength for the structure is known from the study conducted on TPMS structures conducted by Al-Ketan et al. [30]. E, ν, ρ, and the ultimate strength are the only material properties used to represent the core material as shown in Table 4. These key material properties were used in order to increase the accuracy of the model, but they do not provide as much information as the other material models.

Using this data, the ultimate strength was placed into the material properties in

Table 4. TPMS Material Properties

E (Mpa)	800
ν	0.18
ρ ($\frac{kg}{m^3}$)	7.85E+02
Ultimate Strength (MPa)	45

Abaqus for the core material. Although the material properties are not as defined as the others that use Johnson-Cook, Hashin, or Brittle Cracking, it can still provide a useful estimate of how the material will respond. It will be found later in Chapter IV that most of the load on impact is taken by the shell materials opposed to the core.

III. Methodology

3.1 Projectile Impact

Metal matrix composites or cellular metal structures such as the TPMS lattice and how they are used is primarily limited by the method of manufacturing used to create them. Designing a lighter projectile has many benefits when assessing the aircraft weight when carrying thousands of rounds across countless missions but lessens the overall kinetic energy of the projectile. By using a metal matrix composite and TPMS structure made through additive manufacturing, it is possible that a projectile can be manufactured that performs similarly to a solid steel projectile but has reduced weight. The goal of this research was to find how various materials and geometries affected the performance of a projectile that incorporates a sandwich shell layered with materials and additively manufactured cellular structure as the core material. This research focuses on studying the affects of the sandwich shell and what occurs when the casing of the projectiles are altered. In order to study various configurations, an explicit model built in Abaqus/Explicit was used to simulate the projectile impact with the concrete target. Within Abaqus, it is simple to change material properties and orientations from one model to the next. The final step in this research would be to confirm the analysis completed in Abaqus by manufacturing and testing the projectile. By performing this research, it is possible to visualize how creating a new type of projectile shell can impact aircraft weight savings, fuel savings, and how the changes impact lethality of the projectile. [18] [31]

3.2 Sandwich Construction

The projectile casing analyzed within the models is known as the sandwich construction. The casing is comprised of three layers: the outer shell, core, and inner

shell as shown in Fig.17. The outer and inner shells were both made of the same material within each configuration of projectile and were set at a .8 mm thickness. The core of the sandwich construction was made of a lattice structure of inconel 718 and the thickness was 1.6 mm.

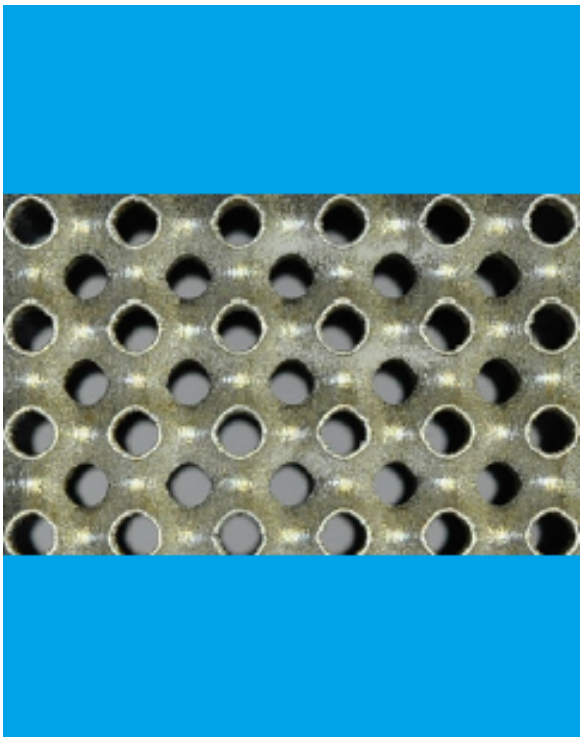

Figure 17. From top to bottom: the outer shell, core TPMS lattice, and the inner shell.

3.3 Triply Periodic Minimal Surface Lattice Structures

The core of the sandwich shell was made from a 3D-printed metal lattice structure using TPMS shown in Fig.18. The TPMS was a sheet-based lattice, meaning the metal within the structure maintains uniform thickness throughout the lattice. By using a TPMS, the casing of the projectile will retain the strength almost as though it were a solid material like the steel projectile. However, the comparative density of the TPMS is far less than if the material was solid. Using material properties derived

from [30], certain assumptions were made for the initial 2D models. First, the TPMS type used was the primitive cell structure with a relative density of 10%. The material properties of the lattice structure were derived using sets of data extracted from Al-Ketan's research as shown in Fig.19. [30] [32]

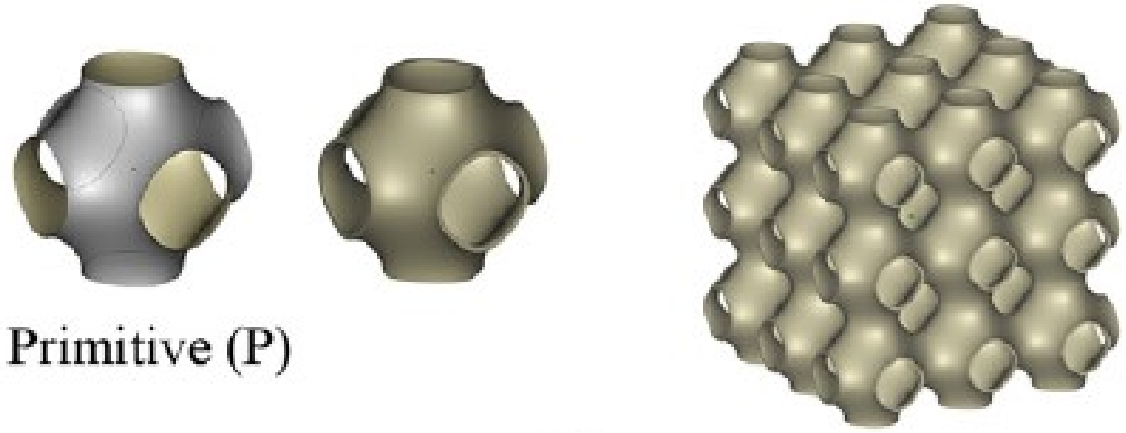

Figure 18. The core material used initially was the Primitive TPMS lattice because of the simplistic design for ease of additive manufacturing. [30]

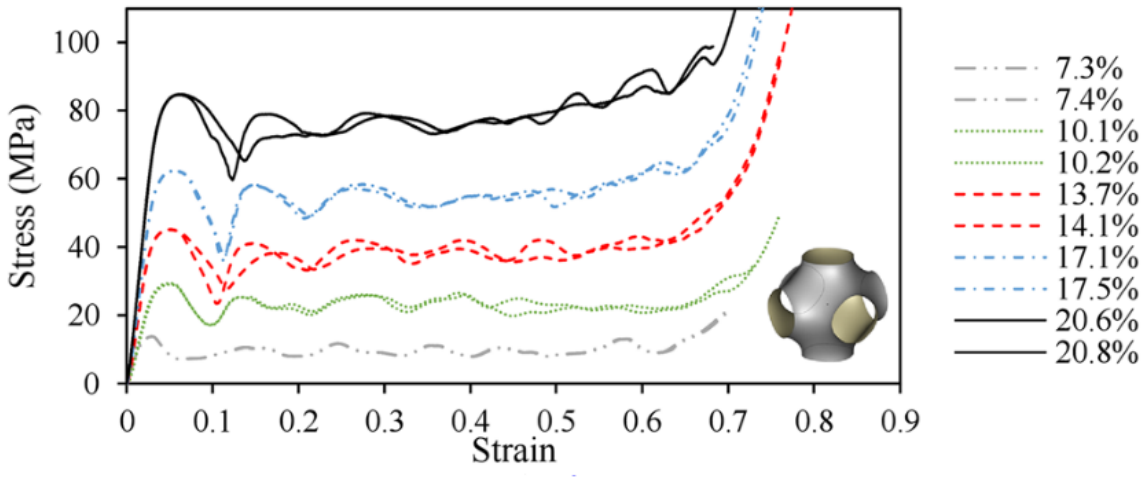

Figure 19. Al-Ketan's study of the relationship between different types of TPMS structures and the relative density of the cells shows how the cell size affects the properties. The primitive cell is shown above. [30]

Based on the findings of Al-Ketan et al., there were multiple TPMS structures that were studied in order to obtain behaviors of each type and how relative density

affects those responses as well. Research is underway in order to find an optimum TPMS structure to use within the projectile as the core, but for this model a primitive structure made of steel at 10% relative density was used. By taking the parameters mentioned, an elastic modulus and density were extracted from the data found in A-Ketan's research. [30]

3.4 Candidates

The following section outlines and describes the candidates for replacing the solid steel casing of the projectile.

Solid Stainless Steel.

A solid stainless steel casing is used as a baseline for observing the changes between the alternate material models. Using the material properties already utilized by Patel, the stainless steel properties are as if the metal was created through additive manufacturing. This is assuming this will be a desirable method for creating such a projectile in the future. The dimensions of the 3.2 mm thick casing projectile are shown in Fig. 44.

Tungsten Shell.

As shown in the preliminary analysis, tungsten-carbide was a desirable metal to use due to a high density, hardness, and stiffness. However, tungsten-carbide is not readily available to be additively manufactured. Tungsten with 5% Nickel was used as a replacement material to be used as an outer and inner shell for the sandwich construction. The properties are still of interest since it is still more dense, harder, and stiffer than stainless steel.

Stainless Steel Shell.

Using stainless steel in conjunction with the inconel 718 lattice structure is also desirable since the whole projectile will be made with less types of materials. This model is the solid stainless steel casing except with the lattice structure replacing the midsection of the casing which lightens the whole projectile.

Silicon-Carbide Reinforced Aluminum.

Silicon-carbide reinforced aluminum (SiCAl) was a composite material chosen for the desirable material properties. Thin layers of the material have high compressive strength in the fiber direction and could be able to transfer the energy from the projectile into the concrete wall without giving to easily. The only problem foreseen in using such a material is that it reduces the weight of the projectile on top of the material reduced by using the lattice structure.

3.5 2D Model Setup

The initial study was done using a 2D plane strain model of a steel projectile and alternate material casing projectiles impacting a concrete target. For simplicity, the alternate material casings were made up of three materials: tungsten, steel, or silicon-carbide reinforced aluminum as the inner and outer shell, a TPMS structure made from inconel 718, and cohesive elements separating those layers. The geometry of both projectiles is shown below. Using Abaqus/Explicit, the concrete wall used in the simulation is 500 mm wide by 500 mm length and is fixed on the top and bottom surfaces during impact. The wall incorporated a brittle failure mode in order to represent the failure of the concrete. For this application, the brittle failure mode provides results closer to what occurs when a high-speed projectile impacts concrete. The model shows cracks forming throughout the concrete during the impact event.

Figure 20. The projectile is modeled after the projectiles used for previous impact projects such as by Provchy and Graves. [7] [8]

When elements fail in the concrete target they are deleted from the model. Although having the elements deleted is not entirely representative of what would happen, the deleted elements represent the pulverization of the concrete aggregate. Similarly, there are elements in the model that do not become deleted but are no longer attached to other elements. The floating or isolated elements represent larger debris that is produced on impact. The various velocities tested were 100, 200, and 300 m/s for each type of projectile. The different projectiles can be compared directly to one another at each velocity, but for the purpose of this paper the 300 m/s case will be the primary focus as all of the noteworthy data occurred at 300 m/s. [9] [15] [16] [21]

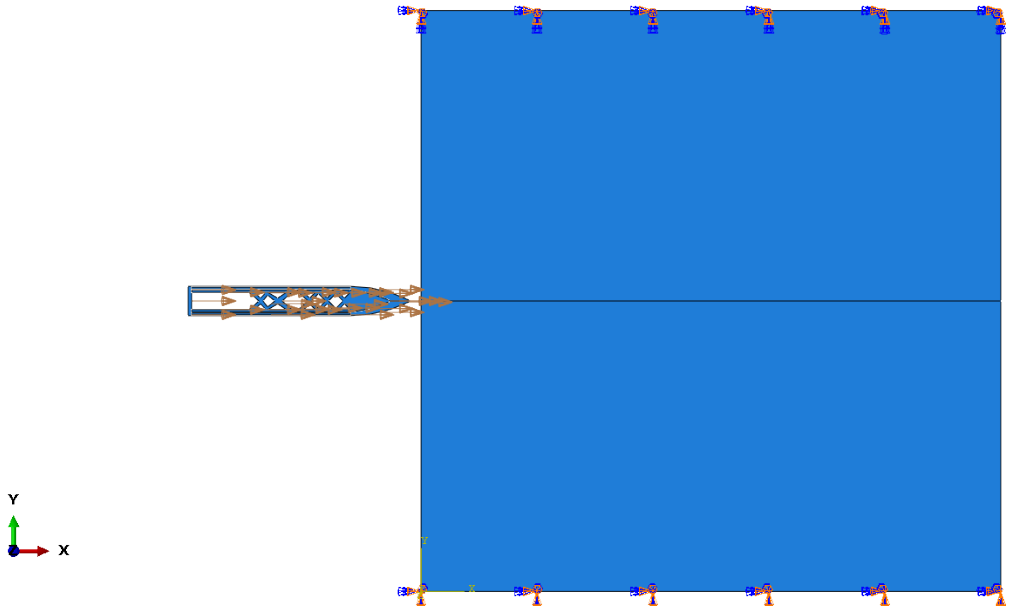

Figure 21. The projectile penetrates the concrete wall from the left at a set velocity. The projectile does not begin to travel while having contact with the wall in order to have proper momentum. The arrows shown in the figure above show the trajectory of the projectile velocity vectors.

3.6 Work Log

The first step in the process was to create an Abaqus explicit model that was an accurate representation of a projectile impacting a concrete target. A 2D dynamic plane strain model was created in order to show how a plane view of the projectile behaved during impact. The plane strain models set up used a steel projectile and a composite casing projectile with unit thickness that impacts a concrete wall. The concrete wall was modeled as a brittle failure model to show how the concrete responds to the impact. Each projectile was run at 100, 200, and 300 m/s and the impact of each was analyzed. Using kinetic energy and seeing how the concrete wall responded to each impact, the model seemed relatively useful for comparing a steel projectile with the composite casing projectile.

The projectile dimensions used were based on previous theses projectiles used. For

this simulation, a sharp-nosed projectile was used since it was one of the projectile nose types used previously. The other nose type that was not used is the ogive nose that is more rounded and might be tested later. A casing thickness of 3.2 mm was used for these projectiles, so the steel projectile has a 3.2 mm steel casing while the composite projectile has a core of 1.6 mm sandwiched by two .8 mm tungsten carbide composite layers.

3.7 Preliminary 2D Results

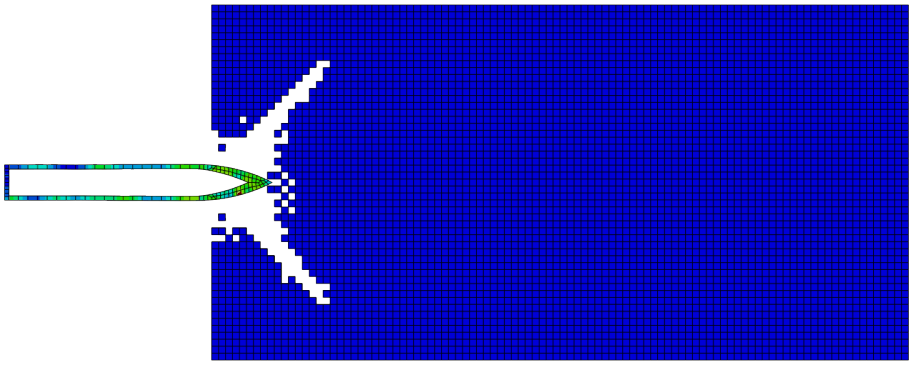

Figure 22. Steel Projectile 100m/s

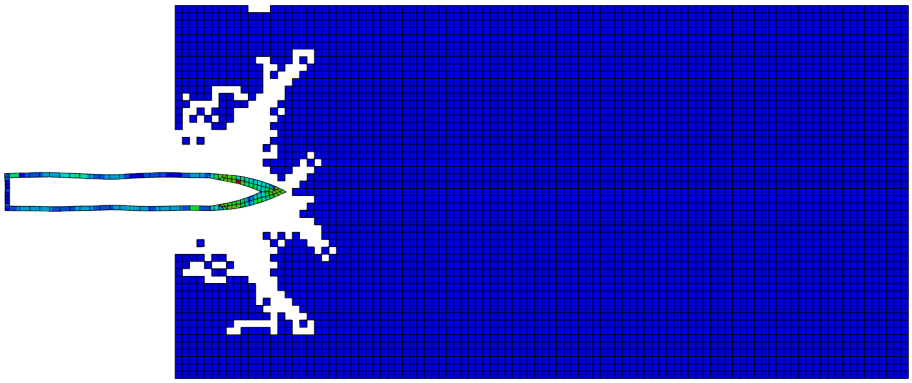

Figure 23. Steel Projectile 200m/s

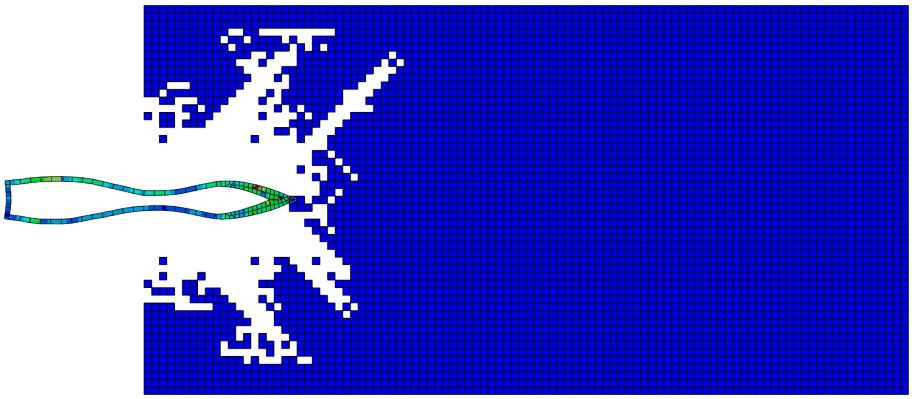

Figure 24. Steel Projectile 300m/s

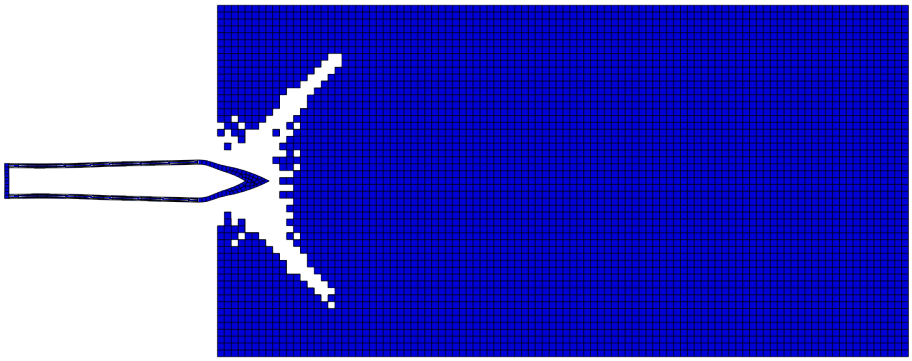

Figure 25. SS Sandwich Projectile 100m/s

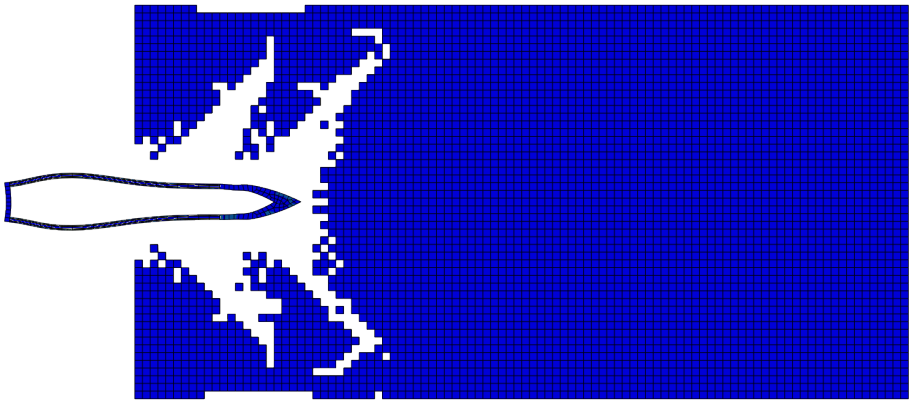

Figure 26. SS Sandwich Projectile 200m/s

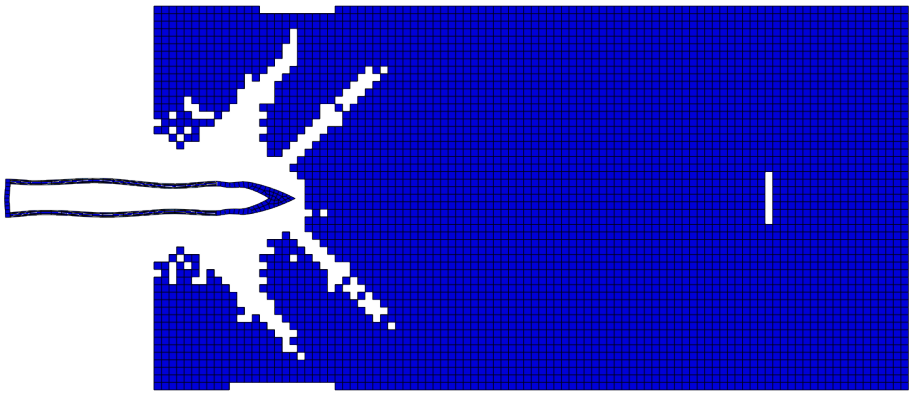

Figure 27. SS Sandwich Projectile 250m/s

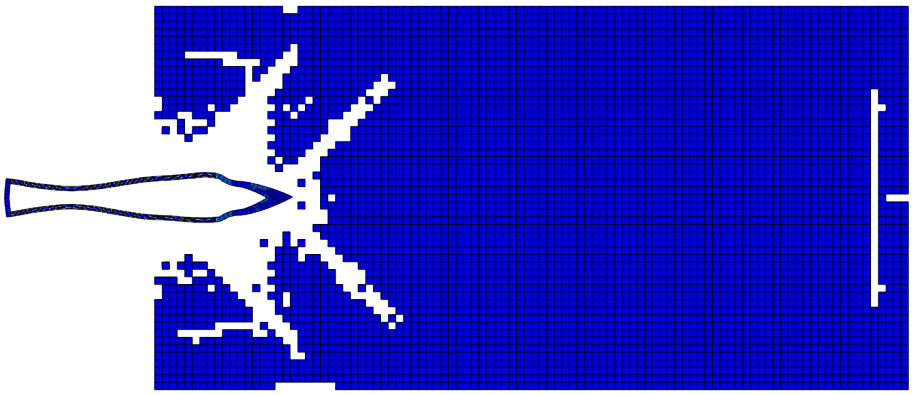

Figure 28. SS Sandwich Projectile 275m/s

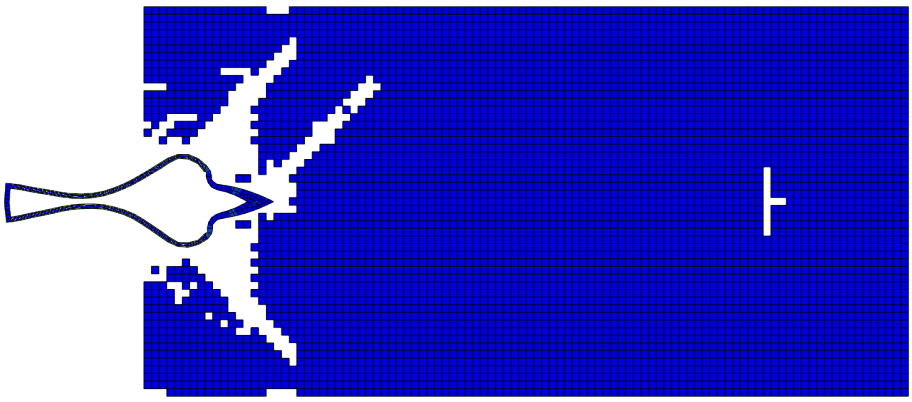

Figure 29. SS Sandwich Projectile 300m/s

Figs. 22-29 were preliminary results that led to creating the final models used for analysis. Initially, the results for various velocities were desired in order to find out at which velocities the projectiles would fail at. Although there were failures seen in some of the models, the approach to analyzing the projectiles changed by simplifying the models in the way they were constructed. After the models were simplified, they were refined by decreasing the size of the elements and the time step while still reaching convergence in the solutions. Final material models were used beginning in the next wave of models shown in Figs. 30-37.

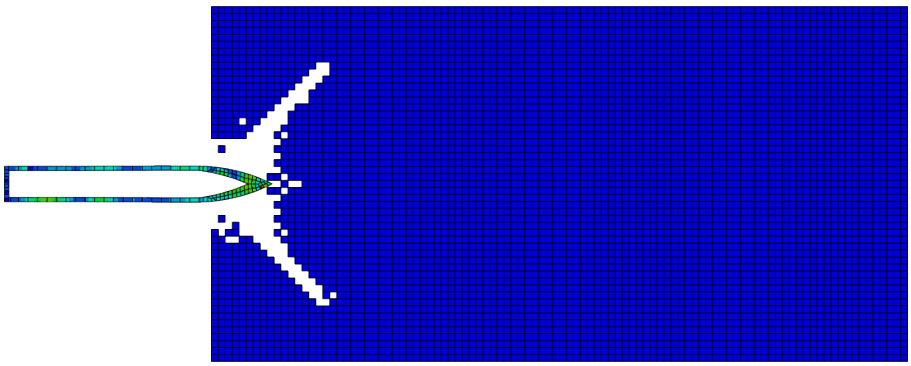

Figure 30. Steel Projectile 100m/s with plasticity.

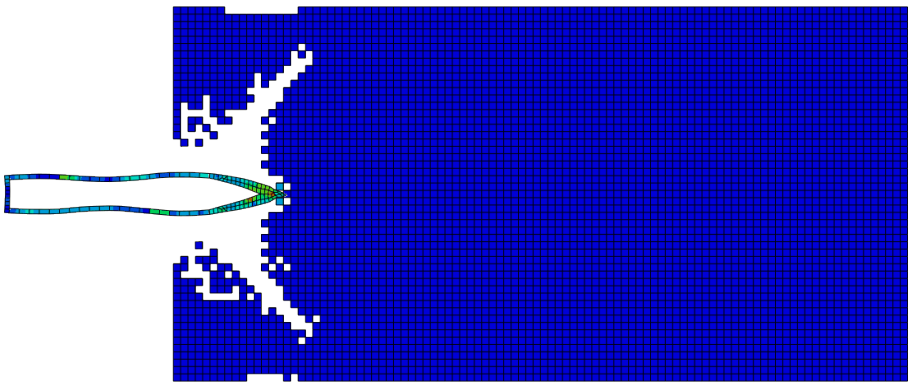

Figure 31. Steel Projectile 200m/s with plasticity.

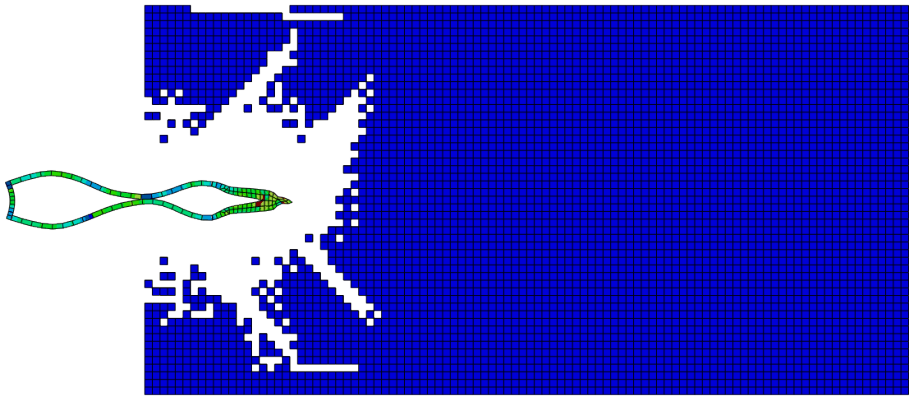

Figure 32. Steel Projectile 300m/s with plasticity.

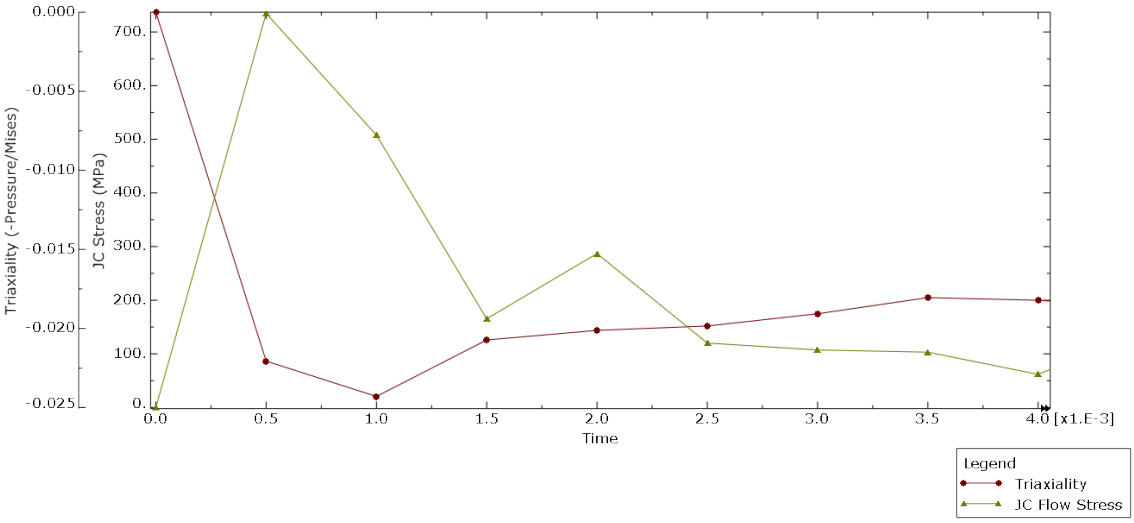

Figure 33. This chart shows the JC data of an element in the nose of the projectile as it is traced through the impact event.

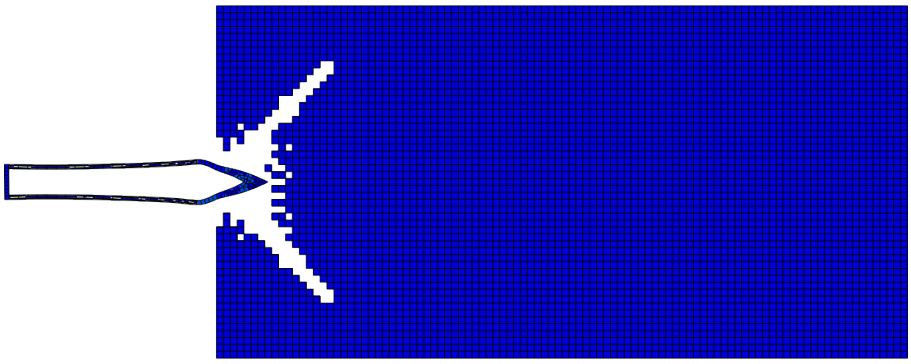

Figure 34. SS Sandwich Projectile 100m/s with plasticity.

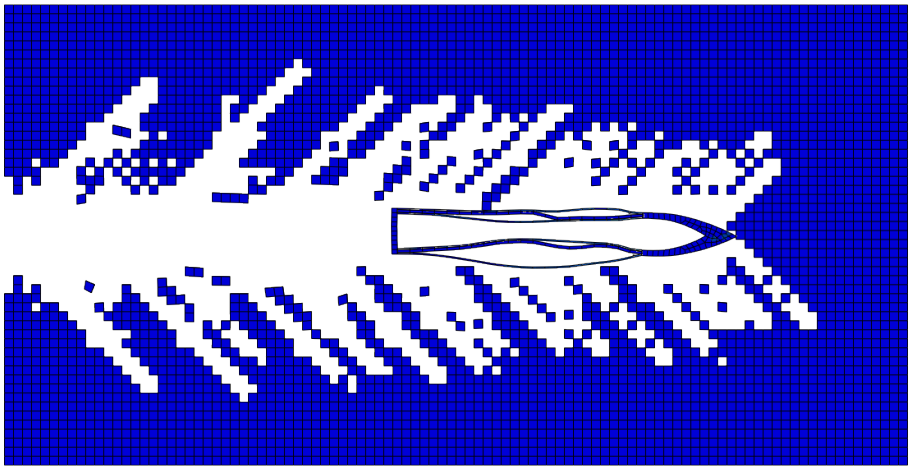

Figure 35. Delamination is shown at .02 seconds after impact of the concrete target using the SS Sandwich Projectile 100m/s with plasticity.

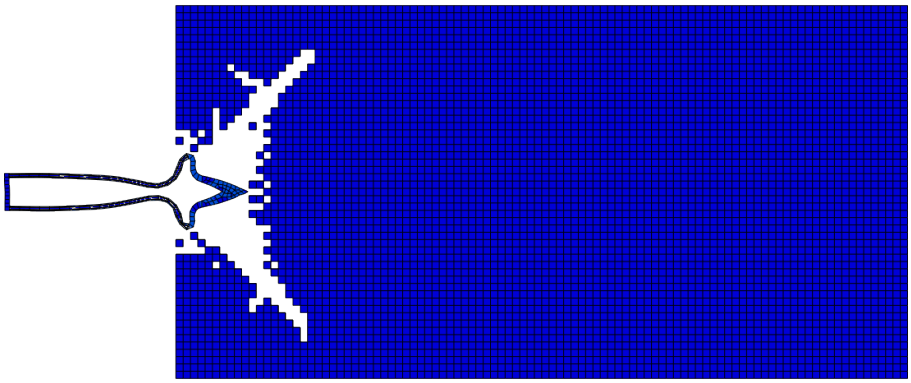

Figure 36. SS Sandwich Projectile 200m/s with plasticity.

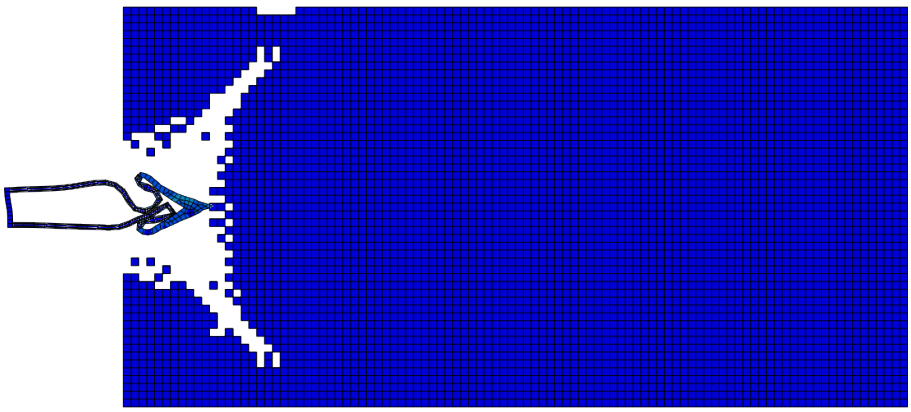

Figure 37. SS Sandwich Projectile 300m/s with plasticity.

Figs. 30-37 show that when JC parameters were added to the sandwich projectile, the survivability of the projectile worsened. The 200 m/s and the 300 m/s both show that the projectile buckles and folds in on itself. Once again the 300 m/s projectile collapsed and did not proceed throughout the concrete, but the 200 m/s projectile did the same. When the sandwich projectile was purely elastic, the 200 m/s projectile performed better than the steel projectile, but with the plasticity added the projectile performed poorly. The steel projectiles with JC parameters added did not affect the performance greatly, but the sandwich projectile looked less feasible. In order to allow the sandwich projectiles to start performing better, it was clear that the internal aluminum lattice must be inserted and attached to the casing to prevent buckling and keep the projectile from failing catastrophically.

Plane Strain Refinement.

The previous models were altered in order to get a more accurate outcome. The concrete wall elements were refined in order to reach convergence of the model and to see a higher definition of the cracks that form on impact. Each of the following figures show iterations of the projectiles that have different casing designs, but all of them have the internal aluminum lattice inserted but not attached to the outer casing. The model was refined so the problem could converge to the most accurate results within reason. Refining the mesh any further would result in models running for days or weeks opposed to just a couple days. The time step for the models used was 1E-06 seconds which allows for an increment that is small enough to allow convergence and show the damage to the various materials involved.

Figure 38. Preliminary SS casing

Figure 39. Preliminary SS casing

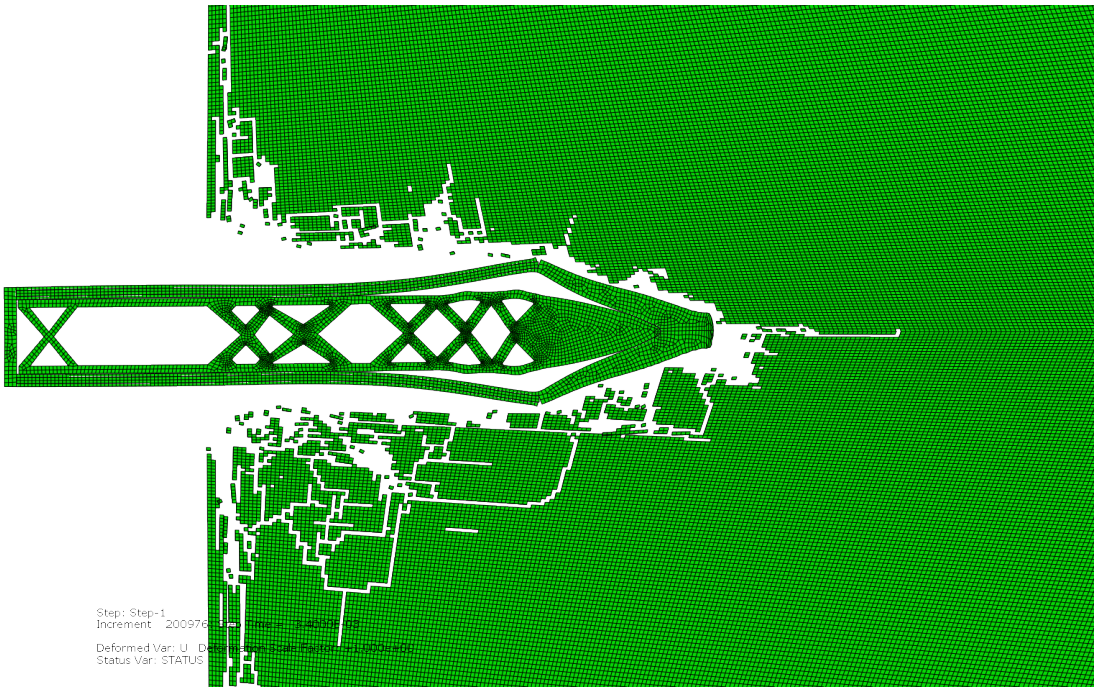

Figure 40. Preliminary SS sandwich casing

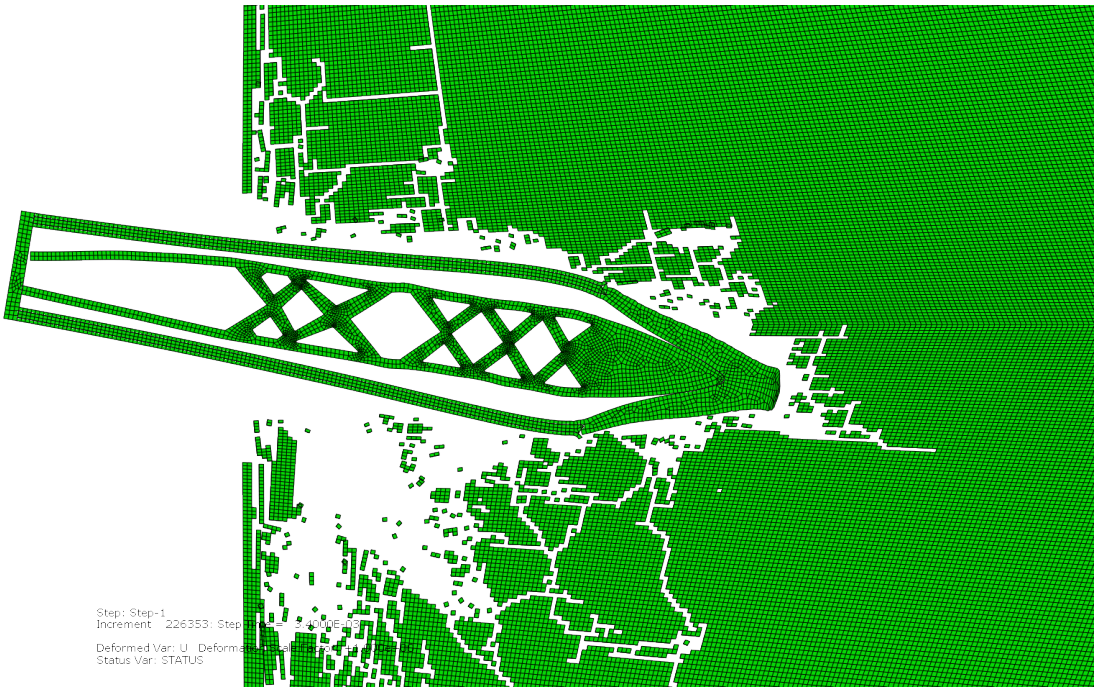

Figure 41. Preliminary tungsten sandwich casing

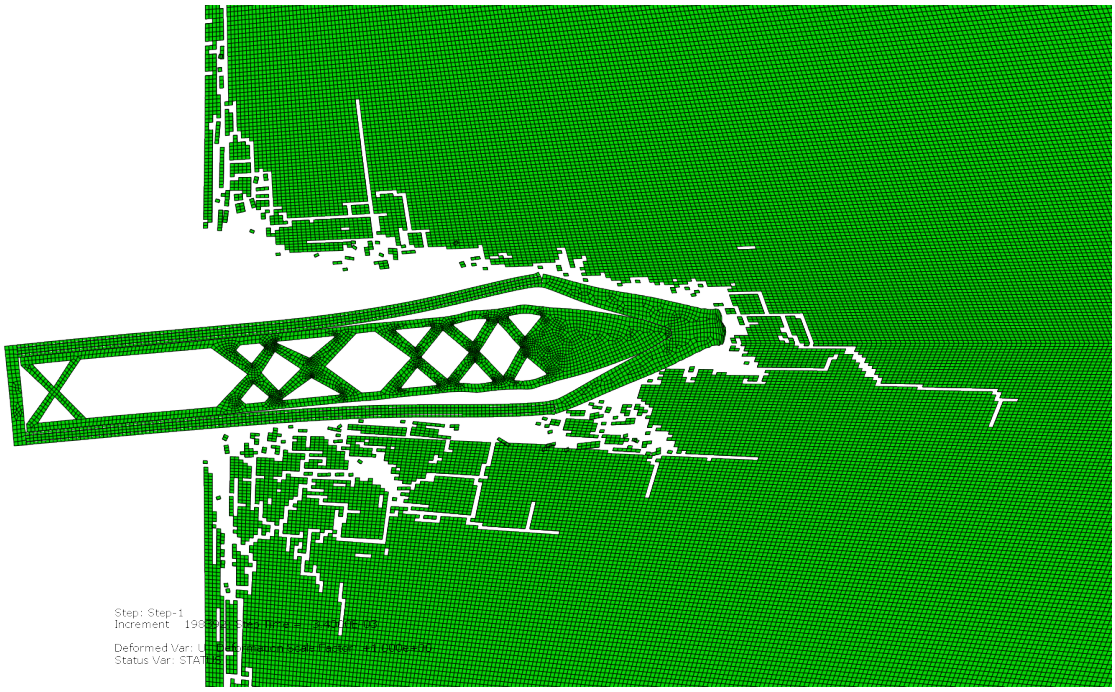

Figure 42. Preliminary SiCAl sandwich casing

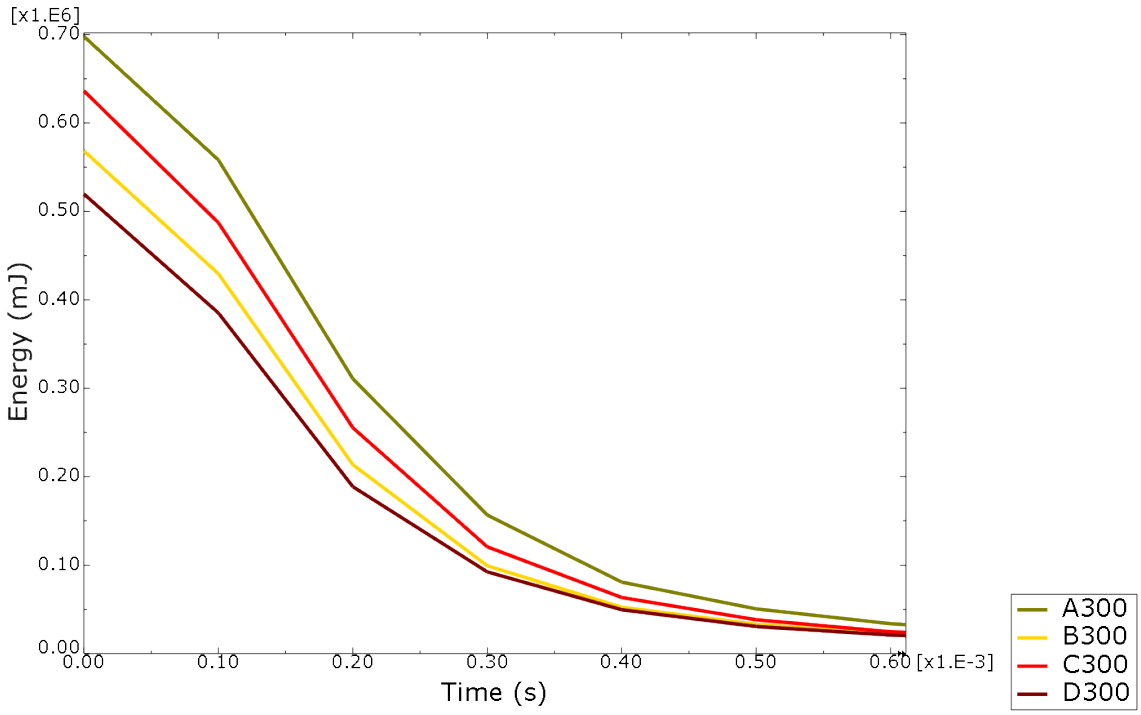

Figure 43. Kinetic Energy of 300 m/s Projectiles. A300, B300, C300, and D300 represented the solid SS casing, SS sandwich, tungsten sandwich, and SiCAl sandwich respectively.

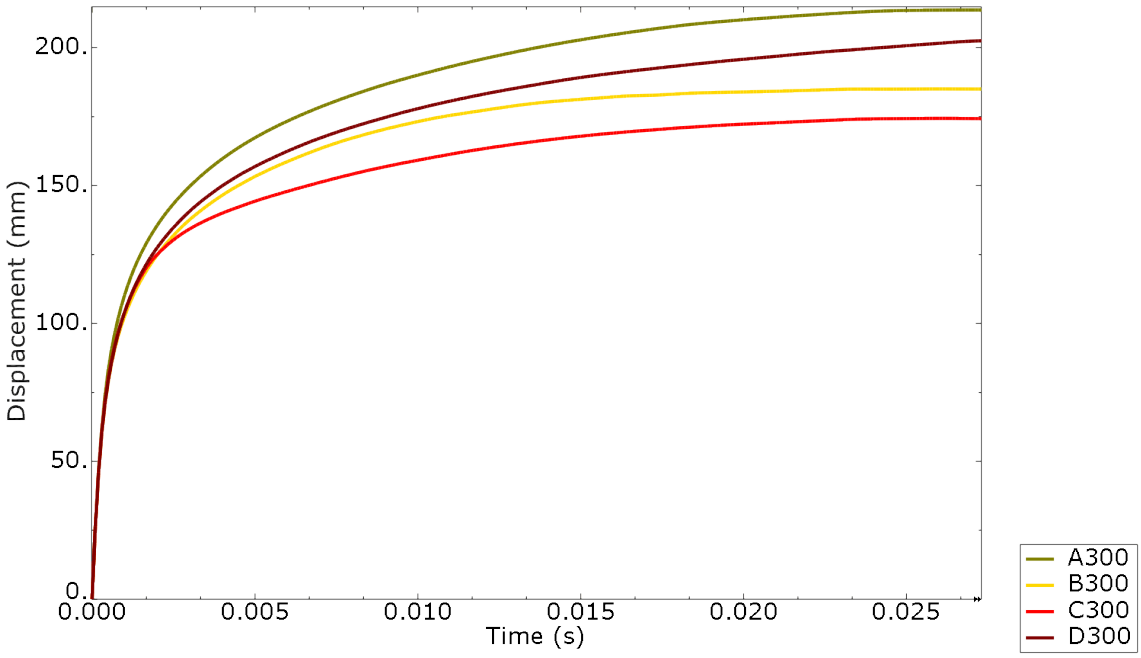

Figure 44. Penetration Depth of 300 m/s Projectiles. A300, B300, C300, and D300 represented the solid SS casing, SS sandwich, tungsten sandwich, and SiCAl sandwich respectively.

3.8 Final Phase

The final iteration of the study came down to looking at the 300 m/s case for seven different configurations of projectiles as seen in Table 5. The RH and RHT versions of the projectile are hollow projectiles with a solid stainless steel casing, while the rest of the versions include the aluminum inner lattice. The IL version includes the aluminum lattice but it is unattached to the casing and the ILA versions include the aluminum lattice but it is attached to the casing. The overarching projectile designs have the following designations: A stands for the solid stainless steel casing, B is the stainless steel sandwich casing, C is the tungsten sandwich casing, and D is the SiCAl sandwich casing. The specifications of each model are shown in Tables 6 and 7. The time step involved with each of the final models was 1E-06 seconds.

Table 5. Seven Final Iterations of Projectiles

Projectile Version	Projectile Model Description
RHT	6.4 mm Solid SS Casing (Hollow)
RH	3.2 mm Solid SS Casing (Hollow)
AIL	Solid SS Casing (Unattached Lattice)
AILA	Solid SS Casing
BILA	SS Sandwich
CILA	Tungsten Sandwich
DILA	SiCAl Sandwich

Table 6. Mesh Specifications For Each Model

	RHT		RH		IL and ILA Models	
Part	Nodes	Elements	Nodes	Elements	Nodes	Elements
Inner Lattice	N/A	N/A	3475	3042	3449	3018
Casing	3122	2772	2028	1681	2686	1747
Wall	162409	161604	162409	161604	162409	161604

For the final iteration, individual elements were traced in order to analyze what was going on within a specific region of the projectile. Fig.45 shows each projectile design with the four traced elements highlighted.

By choosing elements to be traced throughout the impact, the stress wave can be tracked and seen as spikes in the mises stress of the element. Another useful feature is to trace the Johnson-Cook damage within the elements to detect at what point the element fails.

Table 7. Mass Properties of Each Model

Projectile	Mass (kg)	Volume (mm^3)
RHT	1.91E-05	2427.74
RH	1.13E-05	1443.04
AIL	1.55E-05	2957.76
AILA	1.55E-05	2957.76
BILA	1.25E-05	2957.76
CILA	1.41E-05	2957.76
DILA	1.14E-05	2957.76

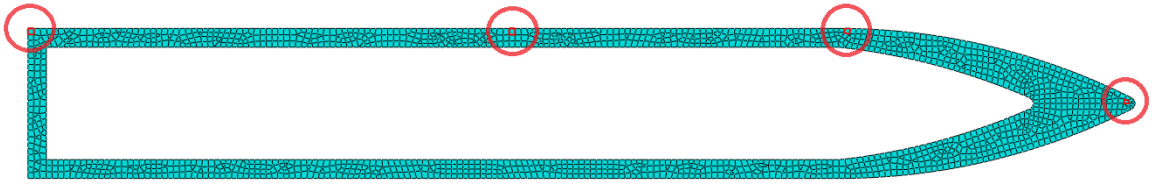

(a) RH Casing

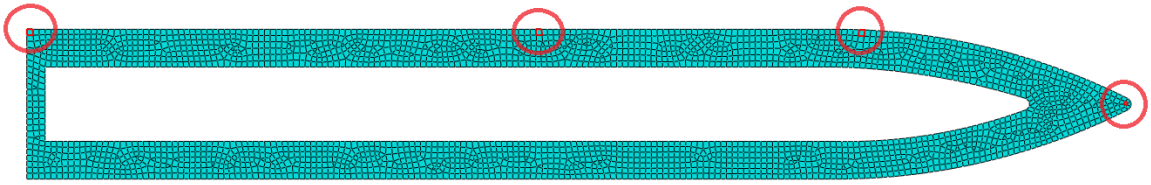

(b) RHT Casing

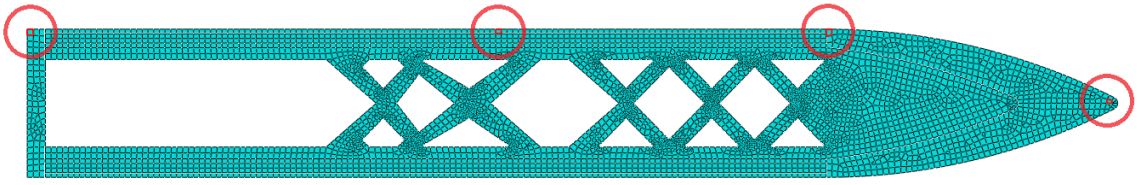

(c) IL and ILA Projectile

Figure 45. Traced Elements in Each Projectile Version. Elements from right to left are E1, E2, E3 and E4.

IV. Results

The following figures outline key points during impact of each projectile design and coordinate with the mises stress vs time figures. The raw data collected and the smoothed data are shown in the first figure for reference, but only the smoothed data will be shown for the remainder of the figures to simplify what is represented.

For Figs. 46 and 47, these two cases can be directly compared because both have similar characteristics but differ in geometry. Fig. 46 shows the hollow 3.2 mm thick stainless steel casing projectile and extreme buckling occurs quickly. It is this case that showcases the need for added reinforcement of the projectile in order not to buckle immediately and experience a catastrophic failure. Fig. 47 shows the hollow 6.4 mm thick stainless steel casing projectile and it serves as the baseline goal for each other projectile version. It clearly penetrates the concrete farther than the 3.2 mm thick casing projectile and it does not experience a critical buckling load during impact. It was clear at this point that if the casing was made 3.2 mm thick, then the projectile would have to survive the impact similarly to the 6.4 mm thick stainless steel projectile. The RH model buckled and the RHT model shows minimal bowing as it impacts the concrete. It is possible that the traced elements within the RHT model experienced much more tension than expected due to the bowing. Since the Mises stress was calculated in each of the traced elements, which could be a cause for some of the unusual results in Fig.48 because the compression in the x-axis became less of a factor due to the tension formed from the bowing. The additional material in the RHT model also adds to the noise experienced by the element since the stress wave scatters throughout the material opposed to being more defined like the RH model shows. The noise within the data is further exemplified by the way the concrete elements fail. As the impact event happens, individual concrete elements fail and disappear from the model. After the elements disappear, the next set of concrete

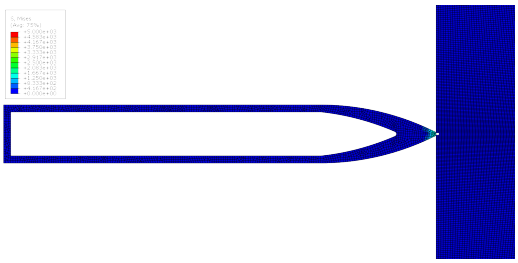

(a) 34 microseconds

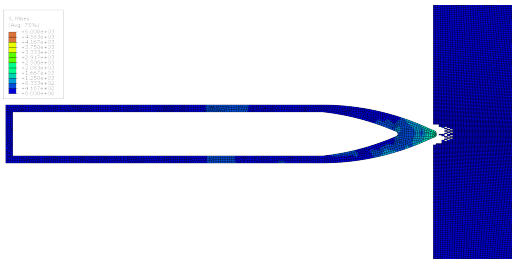

(b) 44 microseconds

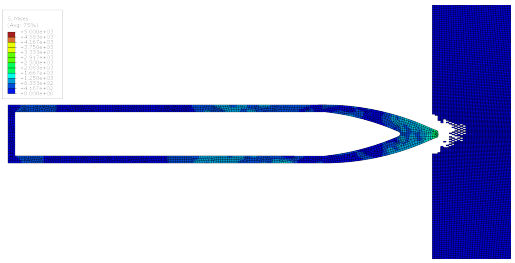

(c) 49 microseconds

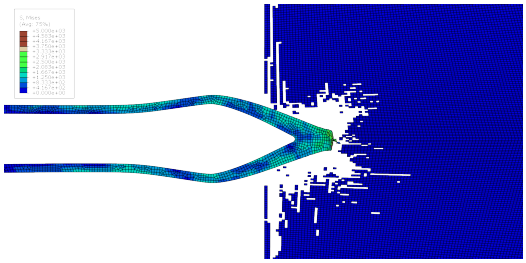

(d) 188 microseconds

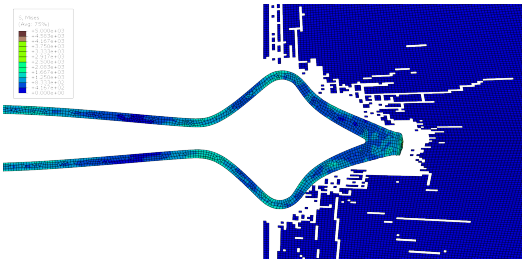

(e) 400 microseconds

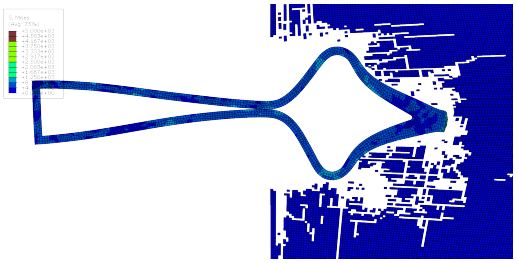

(f) 800 microseconds

Figure 46. RH Projectile During Impact Event. Pictures a-c represent the time step where E1, E2, and E3 first experience the stress wave. Picture d represents when E1 experiences the highest stress value. Pictures e and f are held at constant time increments throughout each model.

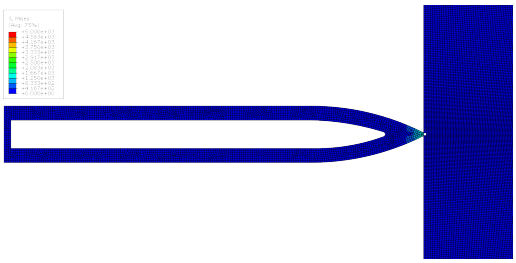

(a) 34 microseconds

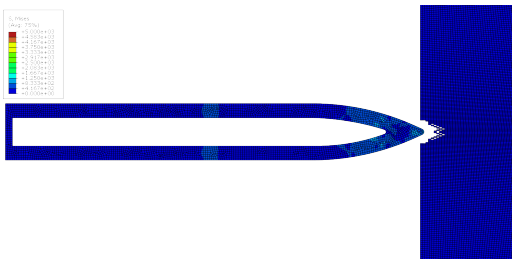

(b) 40 microseconds

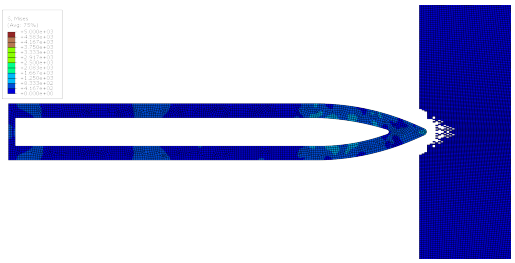

(c) 46 microseconds

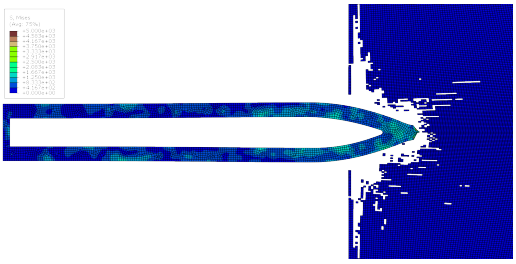

(d) 188 microseconds

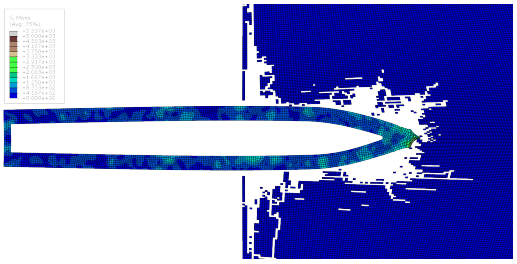

(e) 400 microseconds

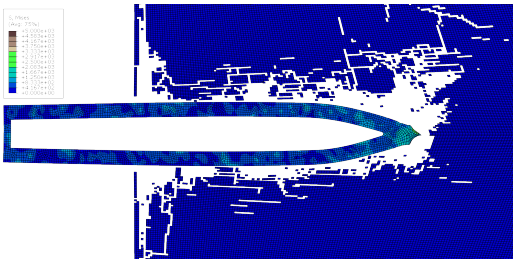

(f) 800 microseconds

Figure 47. RHT Projectile. Pictures a-c represent the time step where E1, E2, and E3 first experience the stress wave. Picture d represents when E1 experiences the highest stress value. Pictures e and f are held at constant time increments throughout each model.

elements become vulnerable to the path of the projectile and will cause an additional stress wave to form when the projectile impacts that set. The pattern of hitting elements, destroying elements, and hitting more elements continues throughout the event which causes more stress waves involved within the projectile and concrete. Fig. 47 shows the stress concentrations are small and scattered throughout the entire part, but Fig.46 shows the stress concentrations are more defined and have less material to travel through. Fig.48 shows how the elements towards the middle of the projectile (E2 and E3) in the RHT model appear to experience half the stress levels shown in the RH model. This result is likely due to the decrease in the thickness of the outer casing from the RHT to the RH model.

The nose deformation of the RHT model is unique amongst the results of the other models. Throughout the impact, the nose of the projectile almost sharpens more than it flattens. Combined with the brittle cracking model for concrete, the sharpened nose could allow the projectile to penetrate further than what is realistic, and it could be a driving factor in the performance of the RHT projectile.

In order to provide more support for the thin casing, an inner lattice was used in the following models to allow the projectile to survive the impact without buckling.

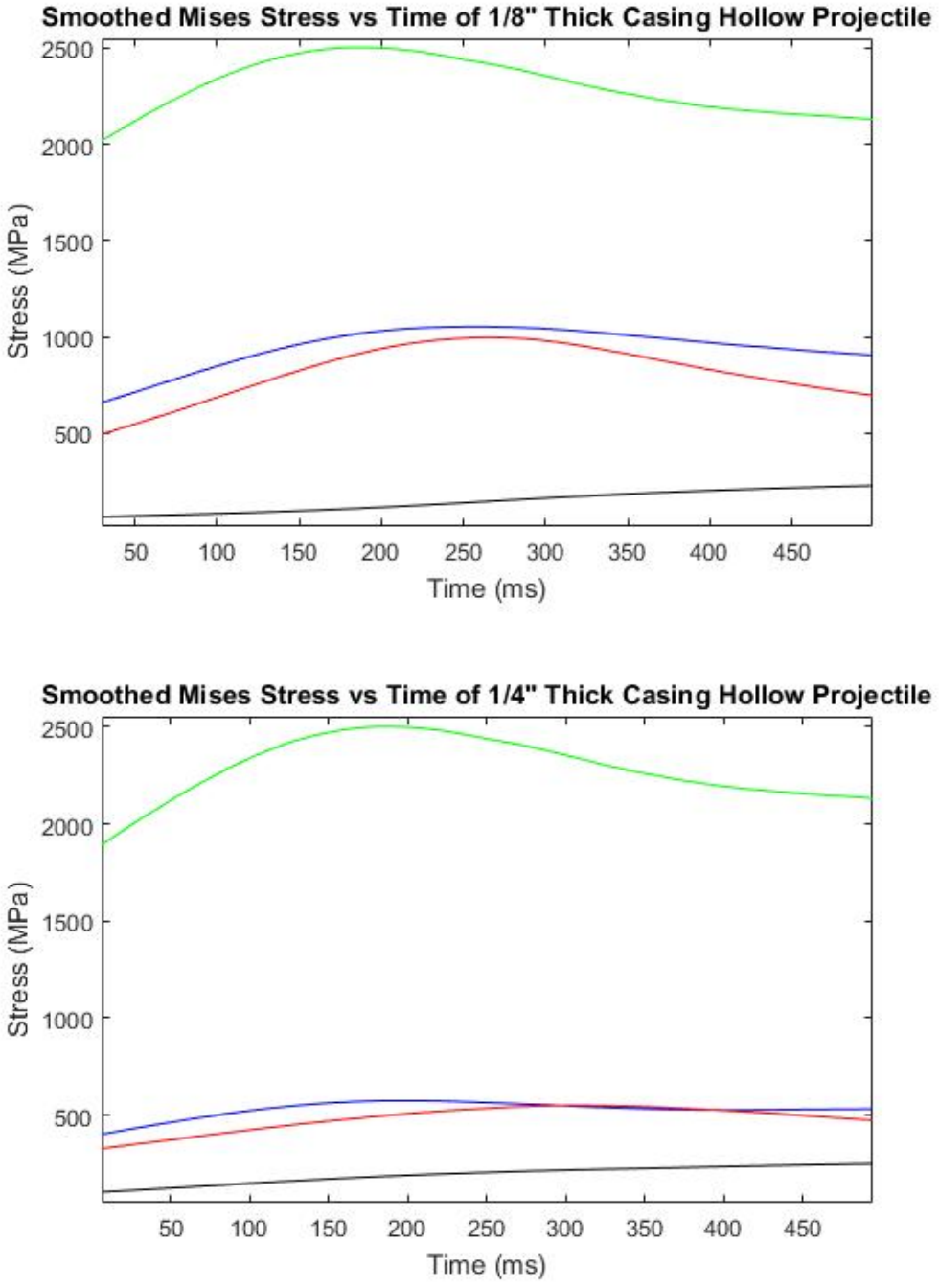

Figure 48. Smoothed Data for RH and RHT Traced Elements. Elements E1, E2, E3, and E4 are represented by the green, blue, red, and black data respectively.

Fig. 50 shows the stainless steel casing projectile with the inner aluminum lattice inserted, but not attached to the outer casing. In this model, it represents the importance of tying the inner lattice to the casing in order to provide extra stiffness and durability of the projectile. Buckling occurs similarly to the hollow stainless steel projectile seen previously and the inner lattice being added adds to the overall mass and kinetic energy of the projectile. Buckling inward did not occur due to the support provided by the internal aluminum lattice. The internal aluminum lattice experiences some buckling shown in Fig. 50 since it takes more of the impact load longitudinally than the other models. Despite the increased kinetic energy, the projectile does not penetrate the concrete as far as the thick casing stainless steel projectile. The need for connecting the inner lattice to the casing is obvious and was conducted for each of the following models.

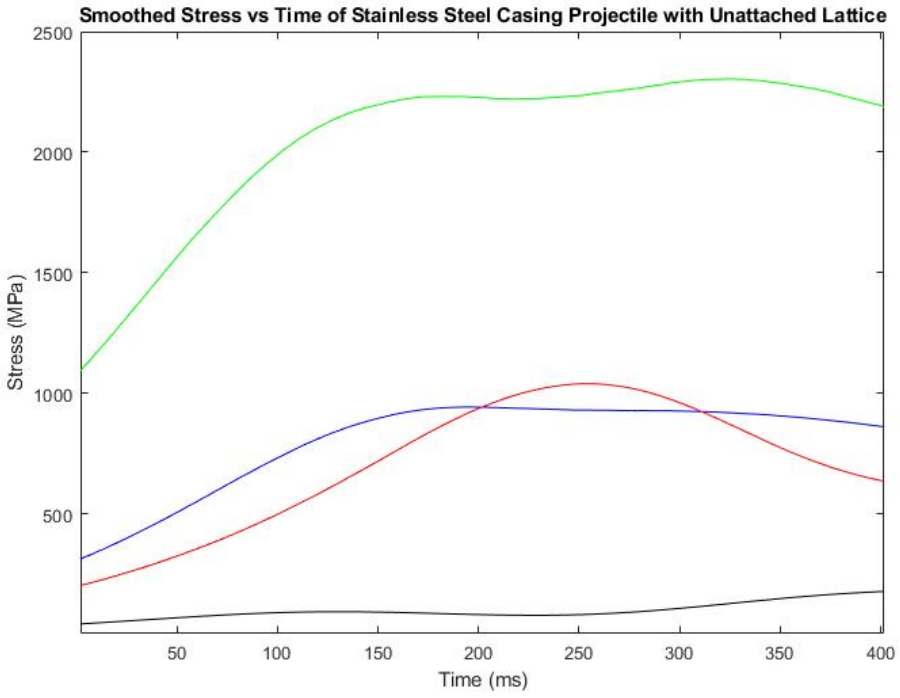

Figure 49. Traced Elements for AIL Projectile. Elements E1, E2, E3, and E4 are represented by the green, blue, red, and black data respectively.

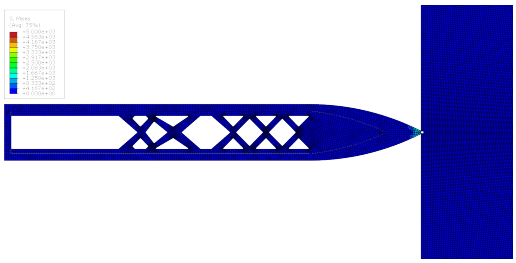

(a) 34 microseconds

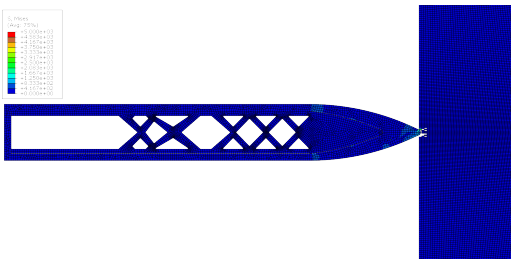

(b) 41 microseconds

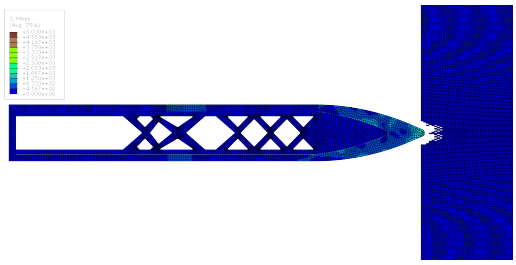

(c) 45 microseconds

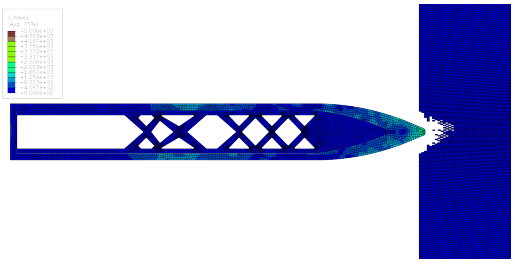

(d) 50 microseconds

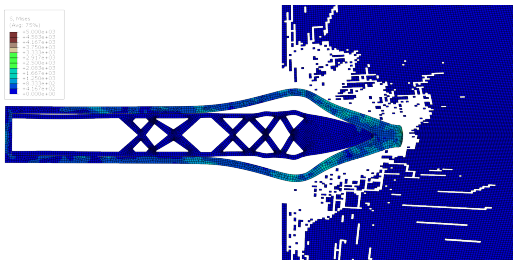

(e) 334 microseconds

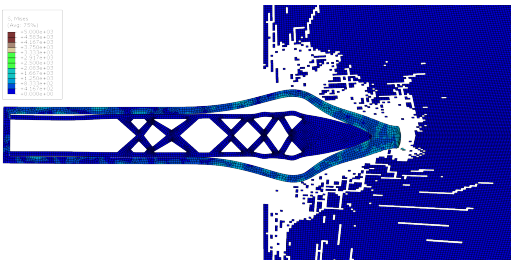

(f) 400 microseconds

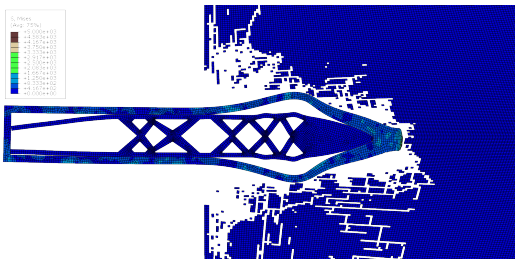

(g) 800 microseconds

Figure 50. AIL Projectile. Pictures a-d represent the time step where E1, E2, E3, and E4 first experience the stress wave. Picture e represents when E1 experiences the highest stress value. Pictures f and g are held at constant time increments throughout each model.

Because of the addition of the inner lattice being attached to the casing, very little to no buckling is present within the model. The inner aluminum lattice effectively adds another layer to the outer casing making the projectile even stiffer than the RHT model. The AILA model penetrates the concrete the most after the RHT model and the results are intuitive. Not only does the model contain the second largest mass out of the seven models, but it also has the inner aluminum lattice tied to the outer casing providing resistance to buckling and increasing rigidness upon impact. The following models show what happens when the sandwich construction is implemented which results in reduced mass of the overall projectile due to the TPMS structure.

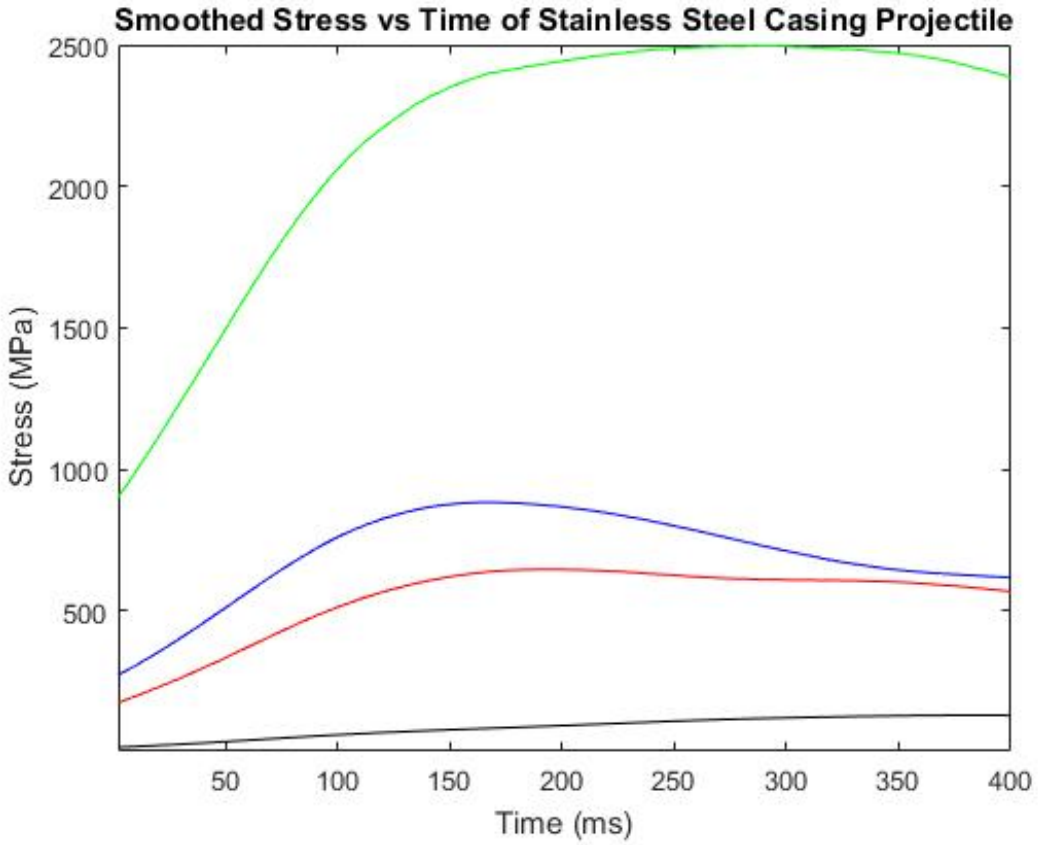

Figure 51. Traced Elements for AILA. Elements E1, E2, E3, and E4 are represented by the green, blue, red, and black data respectively.

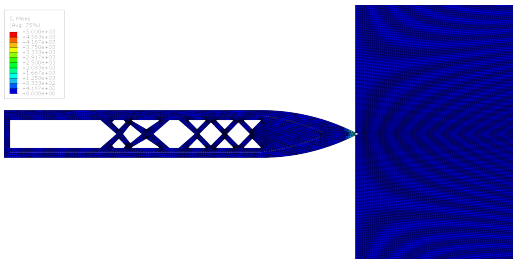

(a) 34 microseconds

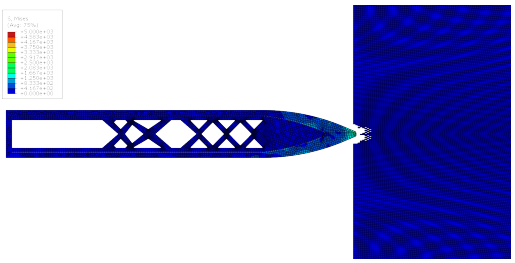

(b) 45 microseconds

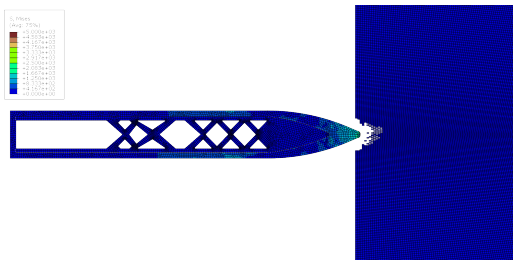

(c) 49 microseconds

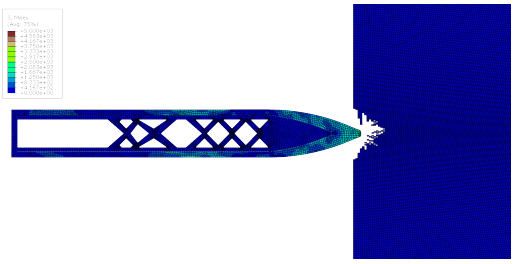

(d) 55 microseconds

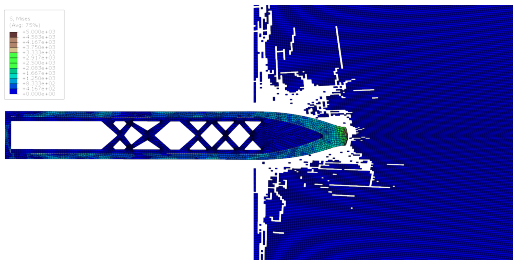

(e) 289 microseconds

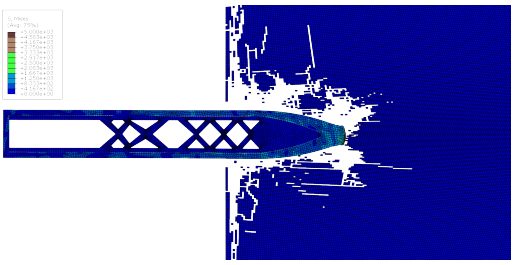

(f) 400 microseconds

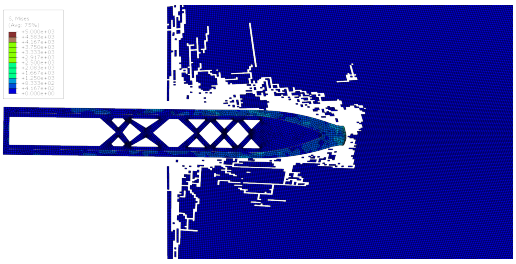

(g) 800 microseconds

Figure 52. AILA Projectile. Pictures a-d represent the time step where E1, E2, E3, and E4 first experience the stress wave. Picture e represents when E1 experiences the highest stress value. Pictures f and g are held at constant time increments throughout each model.

The first iteration of the sandwich construction uses stainless steel as the outer and inner shells, so the projectile is theoretically the same as the previous AILA model except it has a core inconel 718 TPMS layer. As mentioned, the TPMS layer decreases the overall mass of the projectile, so the projectile loses out on some of the kinetic energy involved in the impact. However, the stiffness of the casing can make up for the loss of some of the mass and perform well. The BILA model did not penetrate the concrete as far as some of the previous models, but it outperformed the AIL model which was primarily used to prove the need for an inner aluminum lattice to be attached. From the results, the BILA model was not favorable due to the penetration depth. A suitable replacement for the solid stainless steel casing should perform noticeably better than a model that has buckling such as the AIL model.

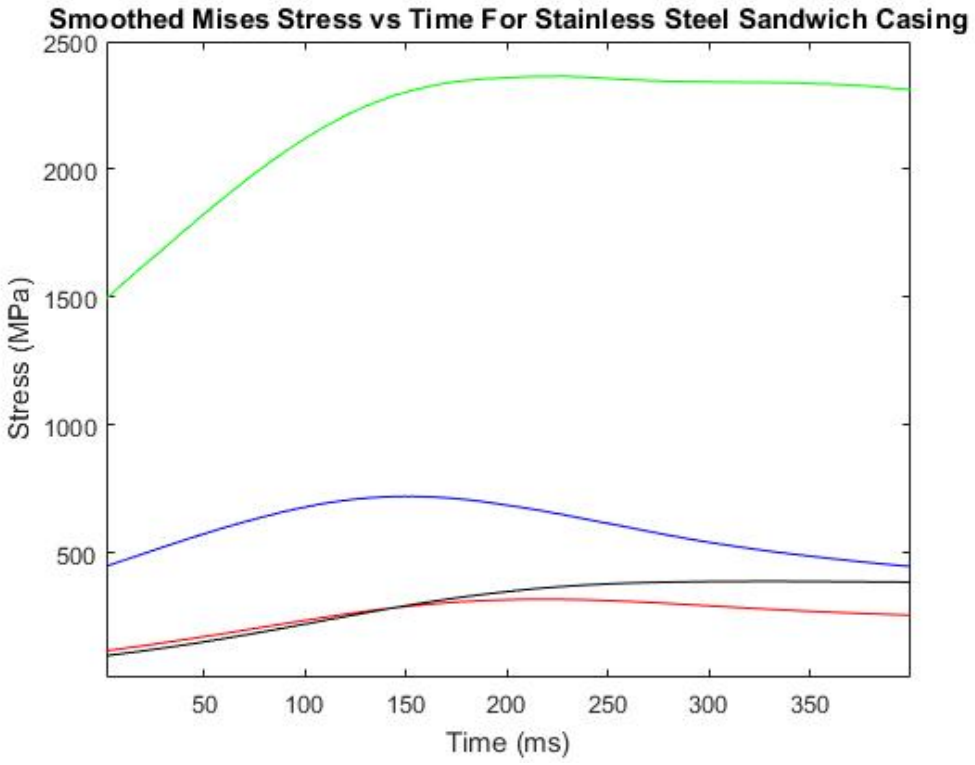

Figure 53. Traced Elements for BILA Projectile. Elements E1, E2, E3, and E4 are represented by the green, blue, red, and black data respectively.

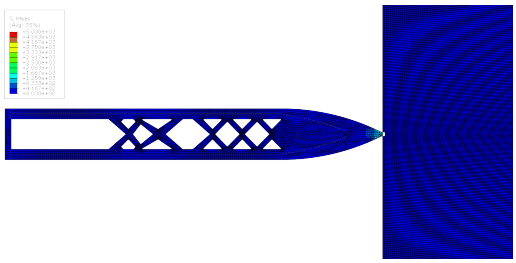

(a) 34 microseconds

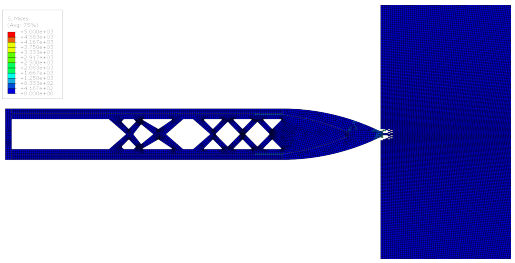

(b) 38 microseconds

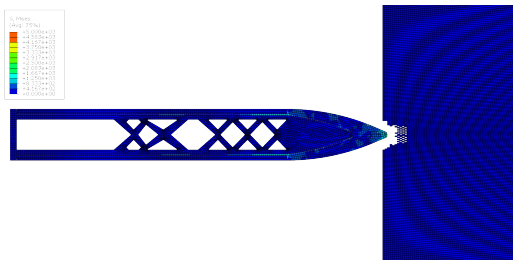

(c) 43 microseconds

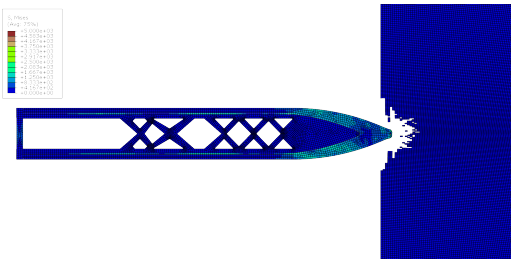

(d) 57 microseconds

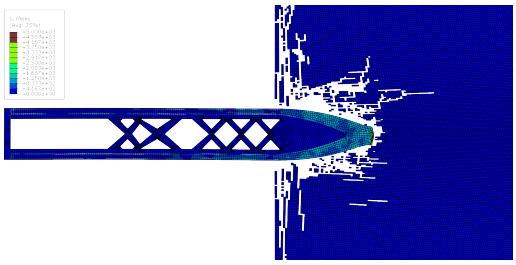

(e) 154 microseconds

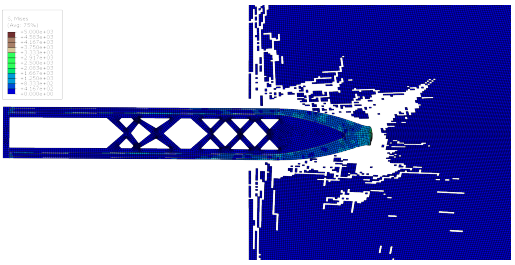

(f) 400 microseconds

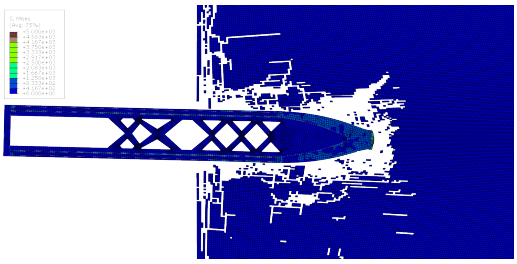

(g) 800 microseconds

Figure 54. BILA Projectile. Pictures a-d represent the time step where E1, E2, E3, and E4 first experience the stress wave. Picture e represents when E1 experiences the highest stress value. Pictures f and g are held at constant time increments throughout each model.

CILA has the tungsten shell for the sandwich construction and the results for this model had a higher level of performance than the BILA model, but comes short of meeting the AILA model in terms of penetration. However, the CILA model performs well despite the reduction in gross mass of the projectile because of the TPMS core. The toughness and stiffness of the tungsten shells make up for the loss in mass and kinetic energy of the projectile and allows the projectile to penetrate further than the BILA model since the stainless steel shells do not add as much mass and rigidness as the tungsten. The results for this model clearly show the importance of the shell material to the overall performance and tungsten is clearly a better option than stainless steel in terms of performance. Note how in Fig.56 the stress wave shows up clearly in the tungsten layers during the impact event. The stiffness and density of the tungsten allow it to take higher levels of stress during the impact and make up for the decreased core material stiffness.

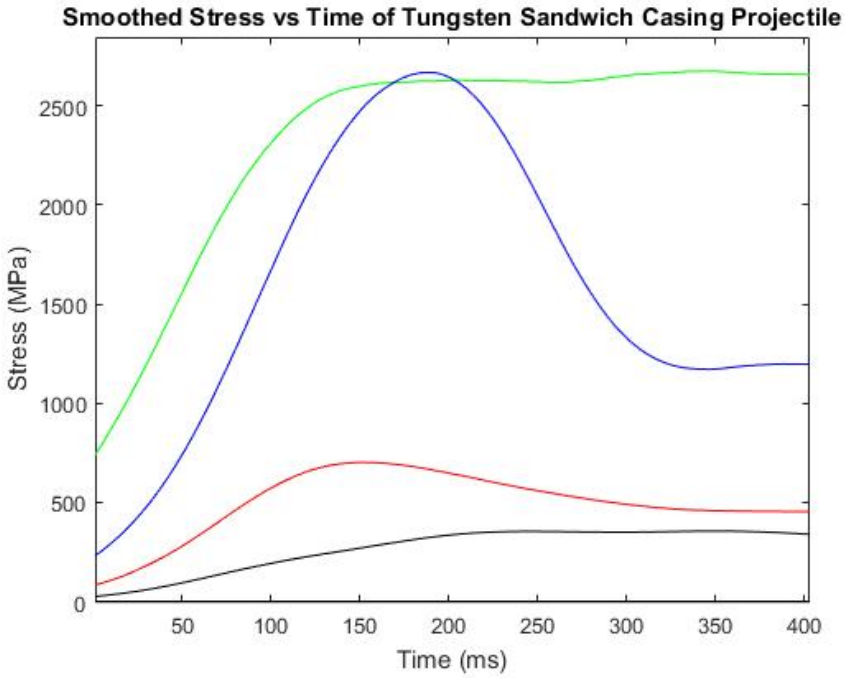

Figure 55. Traced Elements for CILA Projectile. Elements E1, E2, E3, and E4 are represented by the green, blue, red, and black data respectively.

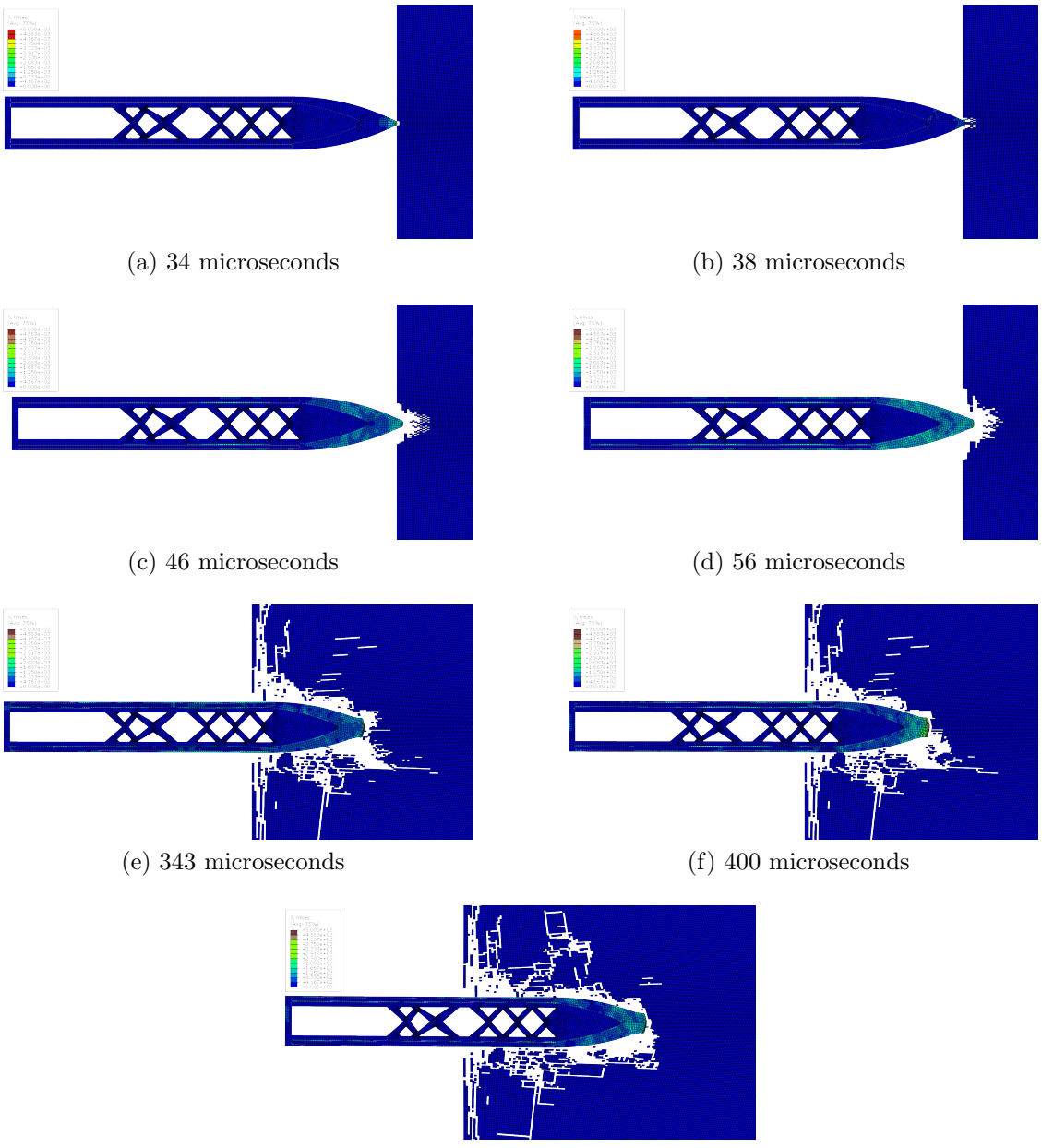

(a) 34 microseconds

(b) 38 microseconds

(c) 46 microseconds

(d) 56 microseconds

(e) 343 microseconds

(f) 400 microseconds

(g) 800 microseconds

Figure 56. CILA Projectile. Pictures a-d represent the time step where E1, E2, E3, and E4 first experience the stress wave. Picture e represents when E1 experiences the highest stress value. Pictures f and g are held at constant time increments throughout each model.

The DILA projectile impacts similarly to the previous projectiles but also shows a bit of a slapping motion near the rear. The slapping motion could be the reason why there is a larger void formed in the concrete above the projectile opposed to below. The asymmetry of the projectile impacts was expected to some degree, but what effects the asymmetry is of interest. It is not clearly visible from Fig.58 that the DILA model penetrates the concrete further than most of the other models, but it still does not penetrate as far as the RHT model. However, what allows the DILA model to compete with the RHT model could be because the stress wave acts longitudinally and transversely as it enters the projectile. The CILA and DILA models' performance levels were on par with one another and that is primarily due to the longitudinal compression strength in the SiCAl. Despite the CILA model having more mass than the DILA model, the DILA model is able to penetrate the concrete just as far as the CILA model because the SiCAl stiffness outperforms tungsten.

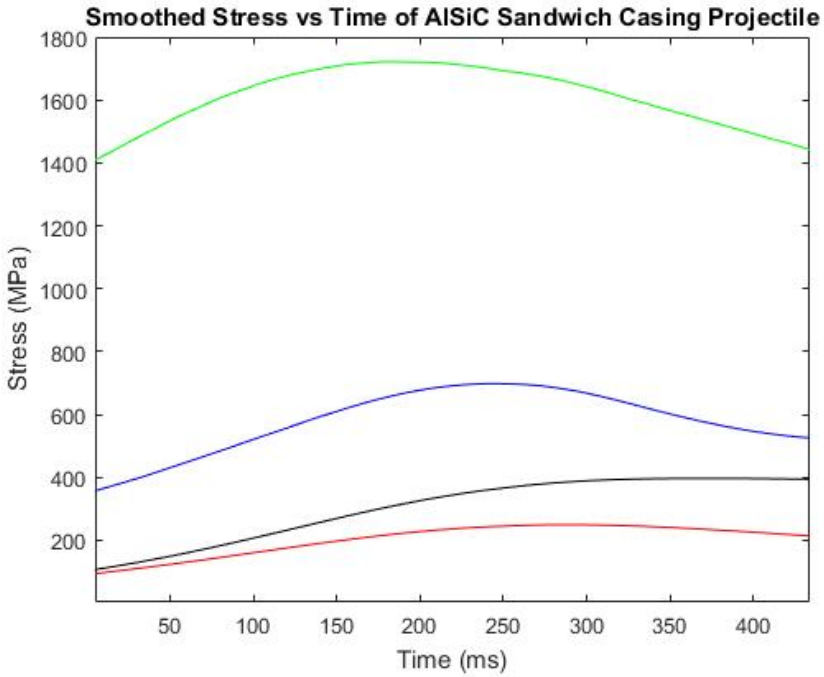

Figure 57. Traced Elements for DILA Projectile. Elements E1, E2, E3, and E4 are represented by the green, blue, red, and black data respectively.

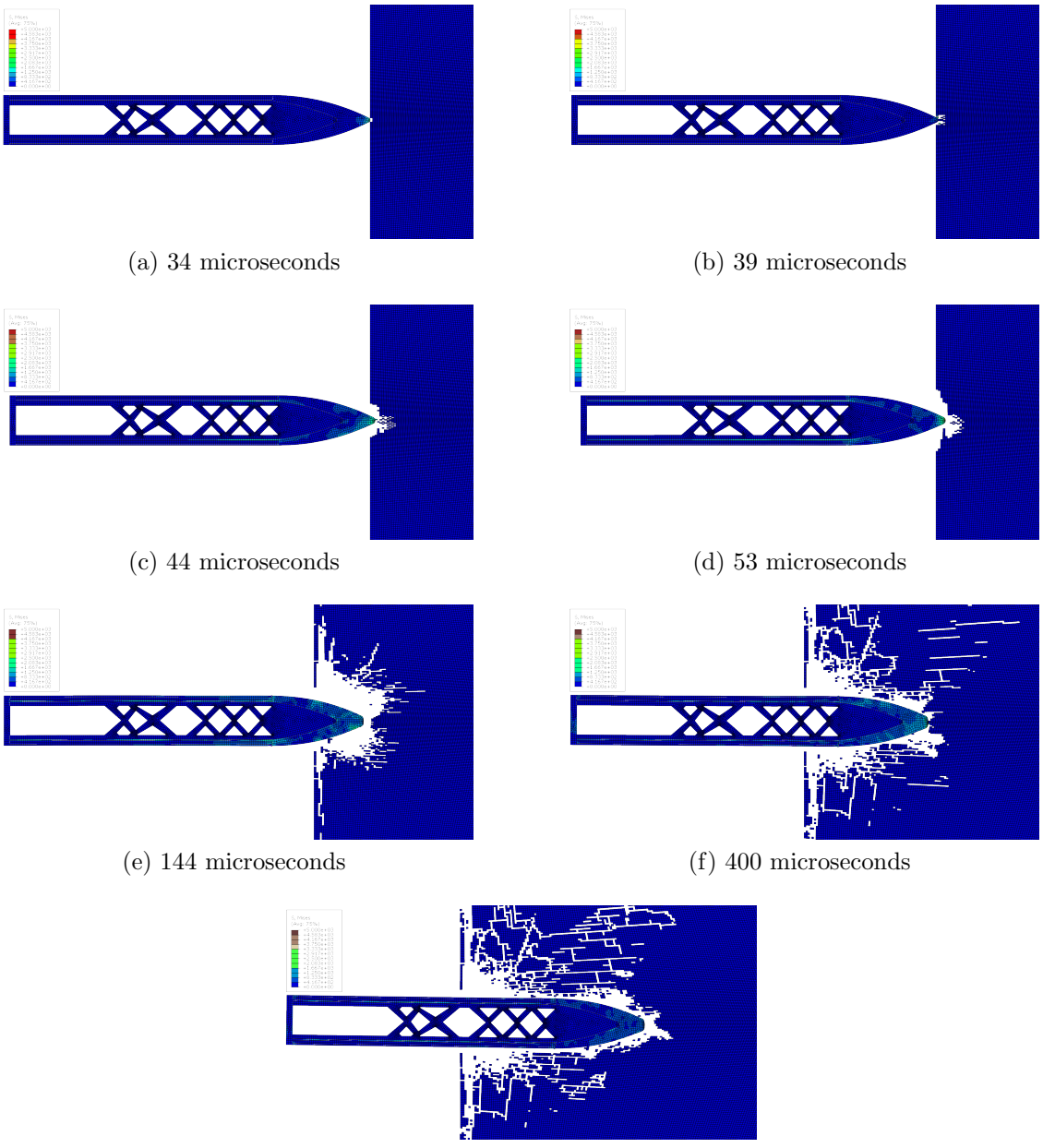

(a) 34 microseconds

(b) 39 microseconds

(c) 44 microseconds

(d) 53 microseconds

(e) 144 microseconds

(f) 400 microseconds

(g) 800 microseconds

Figure 58. DILA Projectile. Pictures a-d represent the time step where E1, E2, E3, and E4 first experience the stress wave. Picture e represents when E1 experiences the highest stress value. Pictures f and g are held at constant time increments throughout each model.

By observing the penetration depth of each projectile model in Fig. 59, each of the versions with the inner lattice attached to the casing performs better than the hollow, thin casing stainless steel projectile and the model with the unattached inner lattice. However, the thick casing stainless steel projectile still penetrates the concrete target the farthest and it destroys the most concrete. Each of the sandwich designs perform similarly which can be expected since each one has similar masses and the differences are based around the shell material which makes up the least amount of material in the whole design. However, the silicon-carbide reinforced aluminum sandwich casing shows that it penetrated the concrete the farthest out of all the versions while having the lowest kinetic energy. The compressive strength of the composite material in the x-axis direction stiffens the casing more than what the tungsten sandwich casing can do, and therefore outperforms the tungsten casing.

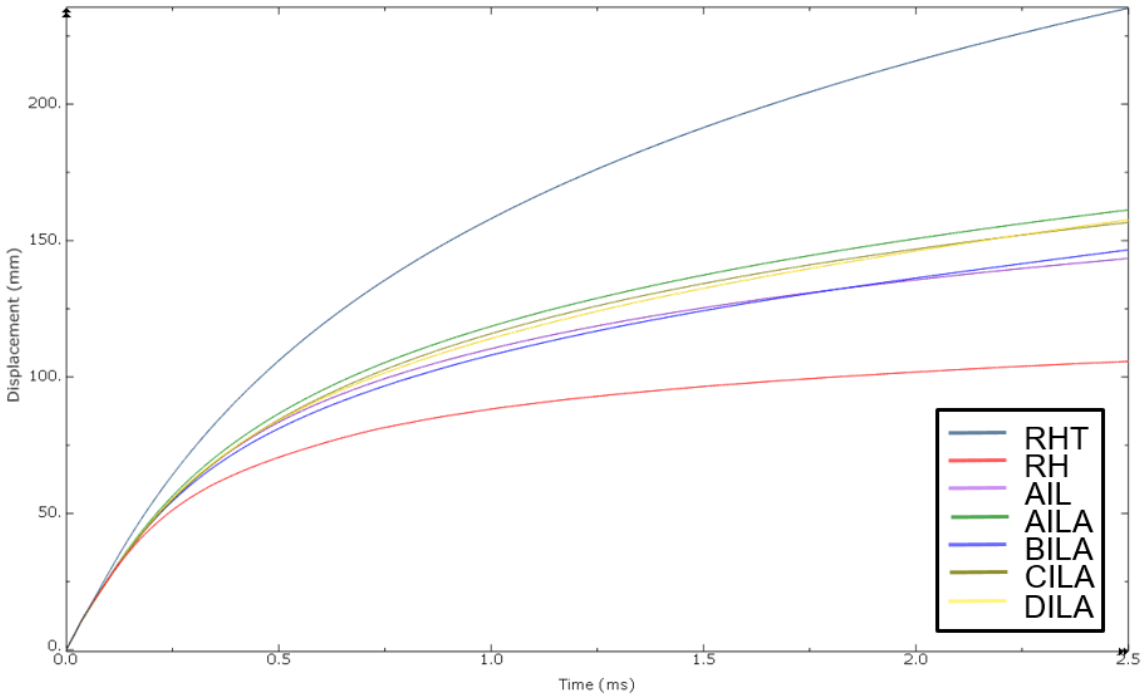

Figure 59. Penetration Depth of the Seven Designs

V. Conclusions and Recommendations

5.1 Preliminary Conclusions

Based on some of the earlier models created using Abaqus/Explicit in order to get to a final solution, it is important to discuss the assumptions made at those stages in the project and how they impacted the final models. The dimensions of the projectile were assumed as shown in Fig. 44 and used roughly the same dimensions as Provchy and Graves used in previous research efforts. One of the main drawbacks of assuming the dimensions and using given lengths, distances, and geometries was the flexibility of this effort to change those. Alternatively, the dimensions were a starting point for the problem and was maintained as one of the fixed variables throughout. Although a change in geometry was not a focus of this effort, other dimensions and shapes of projectiles could be explored further.

When comparing the projectiles shown in Figs. 22-29, it is unclear if one is better than the other in terms of destructive power. While the steel projectiles begin with greater kinetic energy, the 200 m/s sandwich design projectile performed well compared with the steel projectiles. The 300 m/s composite projectile failed to perform anywhere close to any of the other models which was one of the most surprising findings. It would be worthwhile to change how the cohesive elements affect this result and to find out how the bond between the layers makes the projectile perform better or worse. Another variable that could be changed is the core TPMS material since the material, structure type, and relative density can all be altered. The primitive TPMS structure was chosen due to the simplistic construction and relatively similar properties at a low relative density, so changing the type of TPMS structure could be useful.

For the simple plane strain model, mass and material stiffness are clearly driving

factors within the projectile. The sandwich casing was much stiffer than the steel, and the 300 m/s composite projectile likely performed poorly due to the steel nose greatly deforming. A goal for the next analysis would be to extend the composite casing into the nose so the higher velocity composite projectiles could perform better. Also, by extending the inconel core throughout more of the projectile, the projectile becomes lighter which could be detrimental to the lethality, but it would increase the delta between the performance of each of the projectiles.

Fig. 59 outlines the performance of all seven final iterations of models simulated in terms of depth of penetration. The baseline stainless steel casing clearly penetrates farther than any other model ran, so none of the models was able to perform as well as it in terms of penetration depth. The result shows a failure in meeting the overall objective that was set out to be met, but the stages taken along the way during this project helped diminish the gap between performance of the baseline and all other models. Fig. 59 shows that the gaps in performance amongst the models other than the baseline RHT model and the RH model have a small delta between them. Matching the performance of the RHT baseline would likely include increasing the mass of the projectile in some manner, but equally important is to keep the casing as stiff and durable as possible. Perhaps decreasing the size of the inconel 718 primitive TPMS cells could not only increase mass but add to the strength of the casing. Note that by decreasing the size of the cells would make the core material properties closer to solid inconel 718 which is not part of the goal of this project. Altering the core material would have the largest benefits of increasing mass and stiffness, but it also just makes the casing closer to a solid material. Balancing the design, performance, and weight begins to lead towards the need for optimization which was also not the focus of this project.

One of the main goals of the project was to have an MMC as part of the projectile

casing. The DILA model proves that the MMC sandwich can compete with and exceed the performance of the tungsten sandwich. Tungsten was chosen as a potential metal to be used in the design due to the stiffness, hardness, and density which made it a favorable material for a projectile. The final models show the DILA model not only penetrates further than the CILA projectile, but it also weighs less. The SiCAl MMC had at least two positive results over the tungsten sandwich, but the shortcoming of the SiCAl likely comes with manufacturability.

The results found in the final stage of this project are simple and intuitive: a lighter projectile does not penetrate a concrete wall as far as a heavier projectile of the same size and shape. However, a unique sandwich design was proven to be a feasible solution with the aid of an internal lattice which prevents buckling as long as it is tied with the outer casing. A sandwich design projectile can be greatly improved with further research of the outer casing makeup to make it stronger and penetrate further.

5.2 Trouble Areas

Modeling a high-speed impact of a projectile brings many factors into the problem and can cause some issues with attempting solutions. The brittle cracking method used for concrete in this model allowed for a model that ran relatively smoothly compared to the plastic damage models. When running the plastic damage models in Abaqus/Explicit, the classic error of elements becoming too distorted became cumbersome to avoid. The move from a plastic damage model to the brittle cracking damage model nearly eliminated the distorted element errors and made running the simulations much smoother. However, as mentioned previously the brittle cracking damage model is not ideal for modeling high-speed projectile impacts. The problem becomes clear when viewing the collision of the projectile against the concrete wall

as the elements that fail disappear from the model. In some of the models, large groupings of the elements disappear because they have reached the failure strain, but as they disappear there is no material left over to hinder the projectile's movement. As a result, the projectile ends up penetrating more of the concrete than what is realistic.

Also mentioned earlier in the results for the RHT projectile, the nose sharpens more than it flattens out. Every projectile except the RHT model had the nose flatten, and that squished nose likely caused the projectile to have a larger resistance against concrete penetration depth. It is possible that the increase in performance of the RHT projectile could be due to the use of the brittle cracking model which takes the geometry of the projectile into account more highly than the projectile's other responses. Regardless of how the brittle cracking model behaved, the nose deformation likely played a large part in the effectiveness of each projectile.

5.3 Improvements

For the purpose of continuing research on this problem, it is recommended that the axisymmetric model be analyzed using the plastic damage model along with smoothed particle hydrodynamics (SPH). Although the 2D analysis for this problem has merit, a 3D model and a live-fire test to verify would be ideal. A 3D model with SPH was being worked for the purposes of the project, but run-times of models affected the ability to analyze those in addition to the 2D models. The benefits of using an axisymmetric model with SPH is that the impact of the projectile shows the trajectory of the concrete particles as long as the plastic damage model is used for the concrete. If the brittle cracking damage model is used in accordance with SPH, the particles simply disappear from the model and it can be difficult to see what is going on within the concrete. Also as mentioned, the plastic damage model can be

more accurate than using the brittle cracking method.

In order to get a live-fire test ran, the projectile has to be manufactured. The feasibility of manufacturing this projectile was not part of the scope of this project, but considered as to not make it impossible to construct. With the continuing additive manufacturing research being conducted, new techniques for creating parts are being created constantly. It is important that all of the methods of manufacturing these projectiles are considered in order to create a projectile that balances the cost and time to manufacture it along with the performance.

Another key parameter to alter is mass of each projectile in order to test projectiles with similar kinetic energies. By keeping the kinetic energies consistent amongst the models, the results should be able to make the effects of changing materials more clear. Even before test results are gathered, the volumes of each projectile can show how much of a low density material must be added in order to match the mass of a heavy model such as the baseline RHT projectile. It is possible that trying to match the mass of the RHT projectile by adding more material to the sandwich designs may be unrealistic, so more research and thought would have to go into designing such a comparison.

5.4 Concluding Remarks

Designing a new type of projectile is difficult just because why would the design change if what works now is sufficient? The goal was to create something new that has not been done before and see if it can match or exceed the performance of a standard stainless steel projectile of similar size and shape. Although many assumptions were made according to how to model the projectile and concrete as well as using a 2D plane strain model for analysis, the study has merit in that it opens the gateway for exploring these projectile design alternatives. The research highlights what is the

most important factors in designing an effective projectile such as creating a solid bond between an inner structure with the outer casing, using stiff materials for the outer and inner casing shells, and what must be done to match the performance of a much heavier baseline projectile. By using these findings as stepping stones, an axisymmetric model can add to the rigor needed to prove the design can function similarly to a standard projectile. It may be that a lighter projectile will not penetrate a concrete target as well as a heavier one, but the trick is finding a balance between a yield in weight savings vs destructive power necessary for mission success.

Appendix A. Raw and Smoothed Mises Stress Plotted for Element Tracing

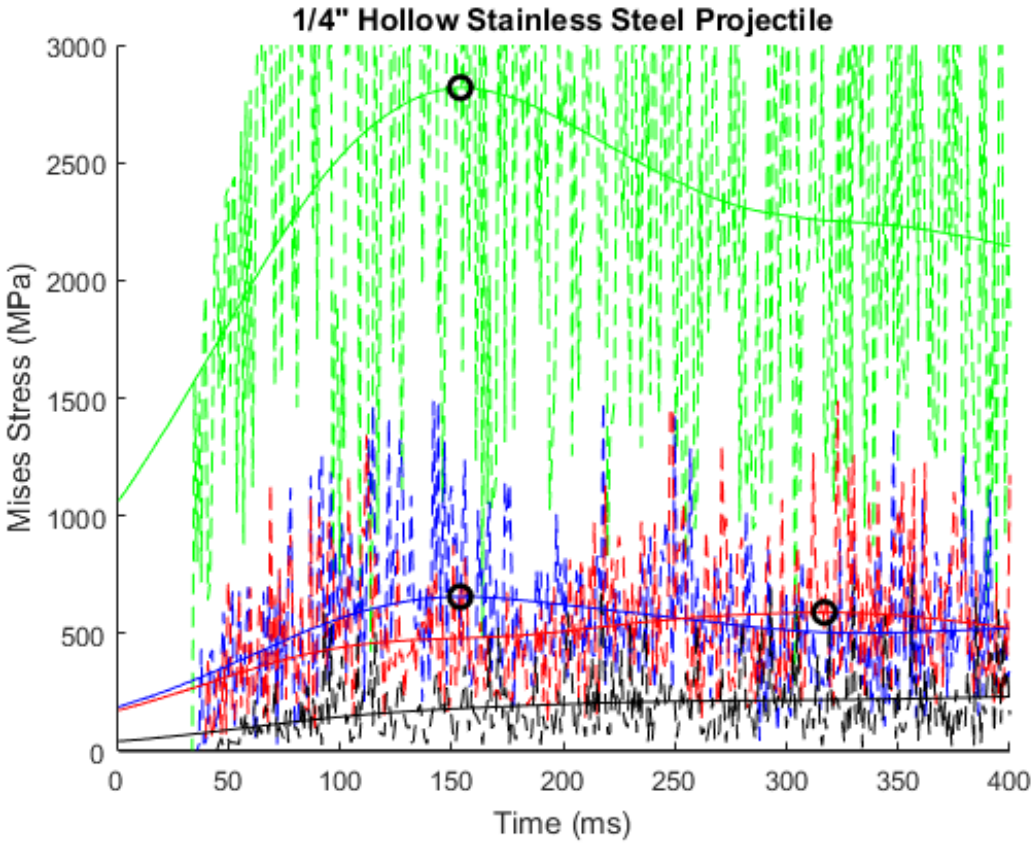

Figure 60. Raw and Smoothed Data for RHT Traced Elements.

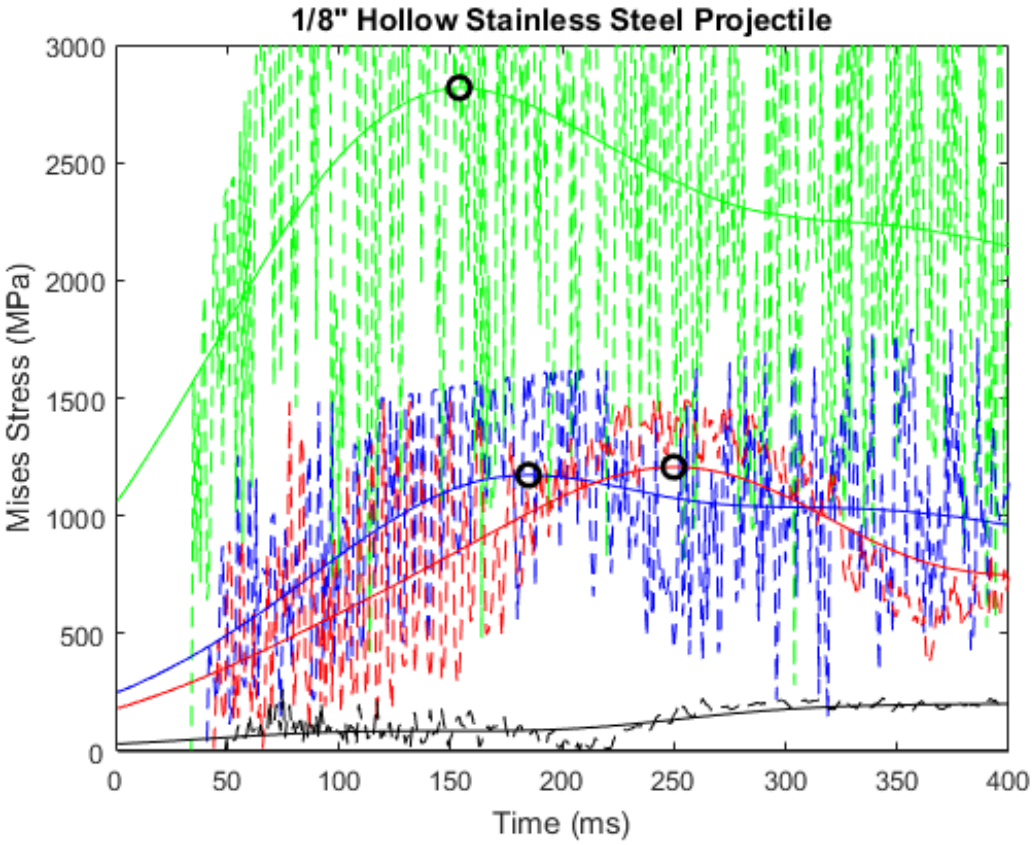

Figure 61. Raw and Smoothed Data for RH Traced Elements.

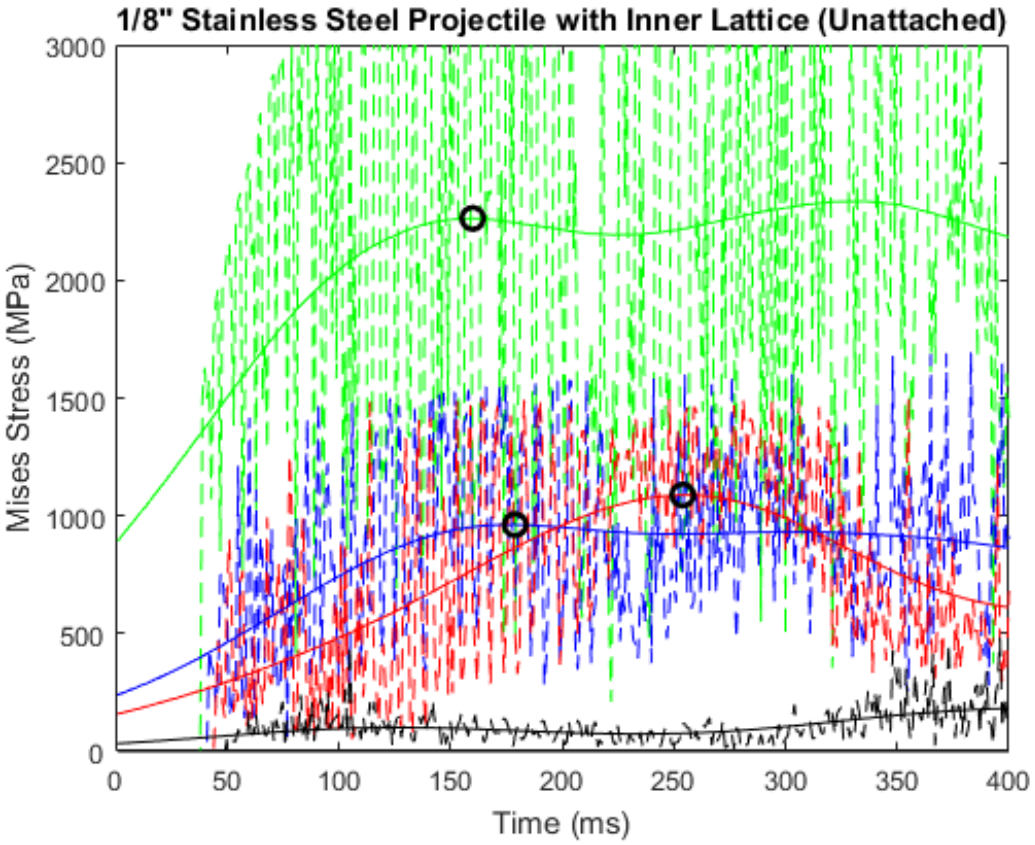

Figure 62. Raw and Smoothed Data for AIL Traced Elements.

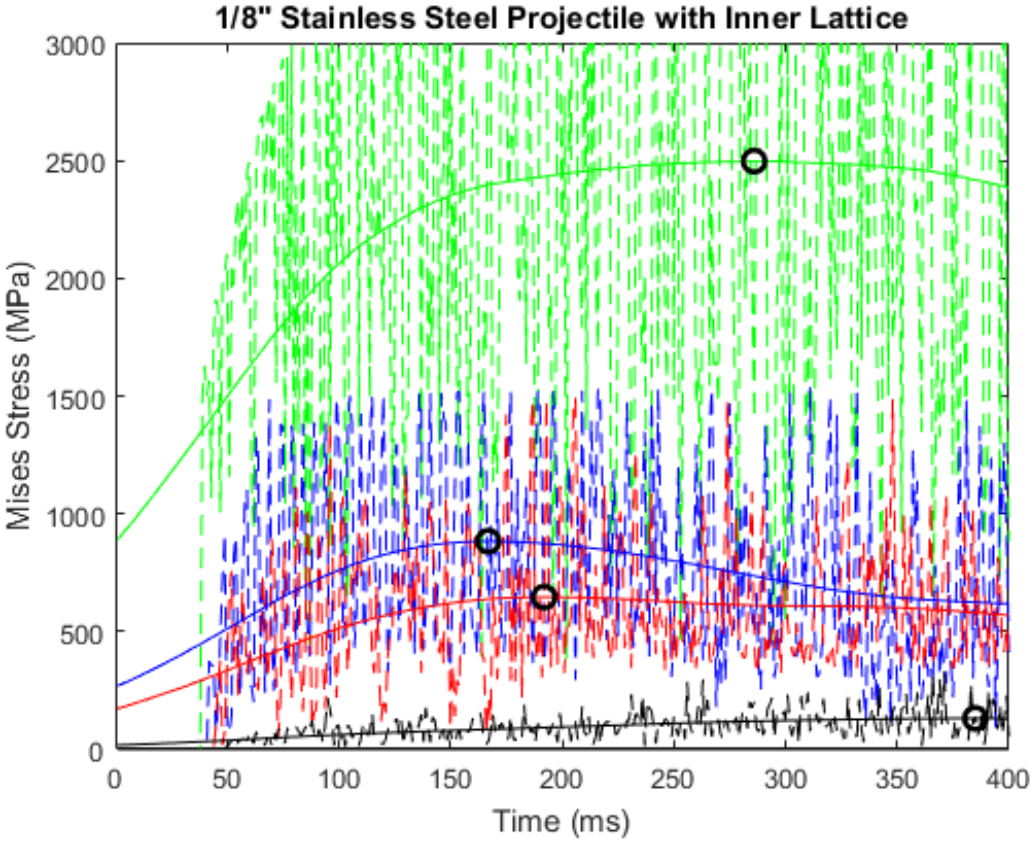

Figure 63. Raw and Smoothed Data for AILA Traced Elements.

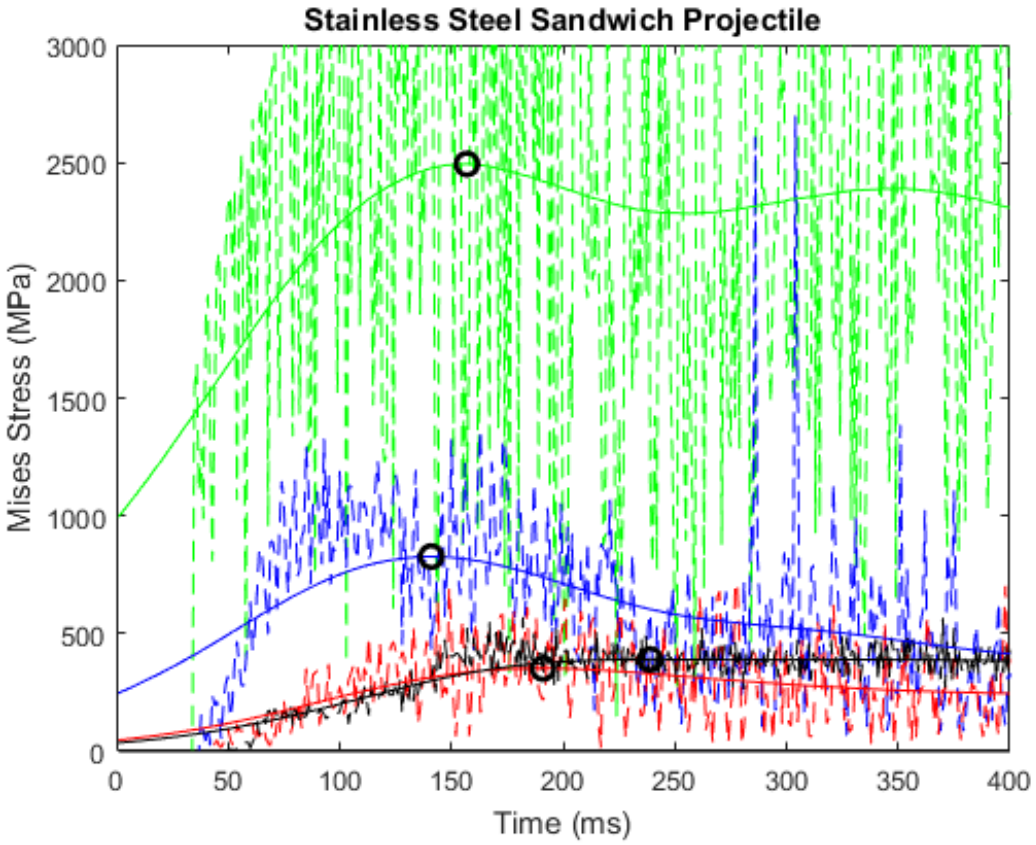

Figure 64. Raw and Smoothed Data for BILA Traced Elements.

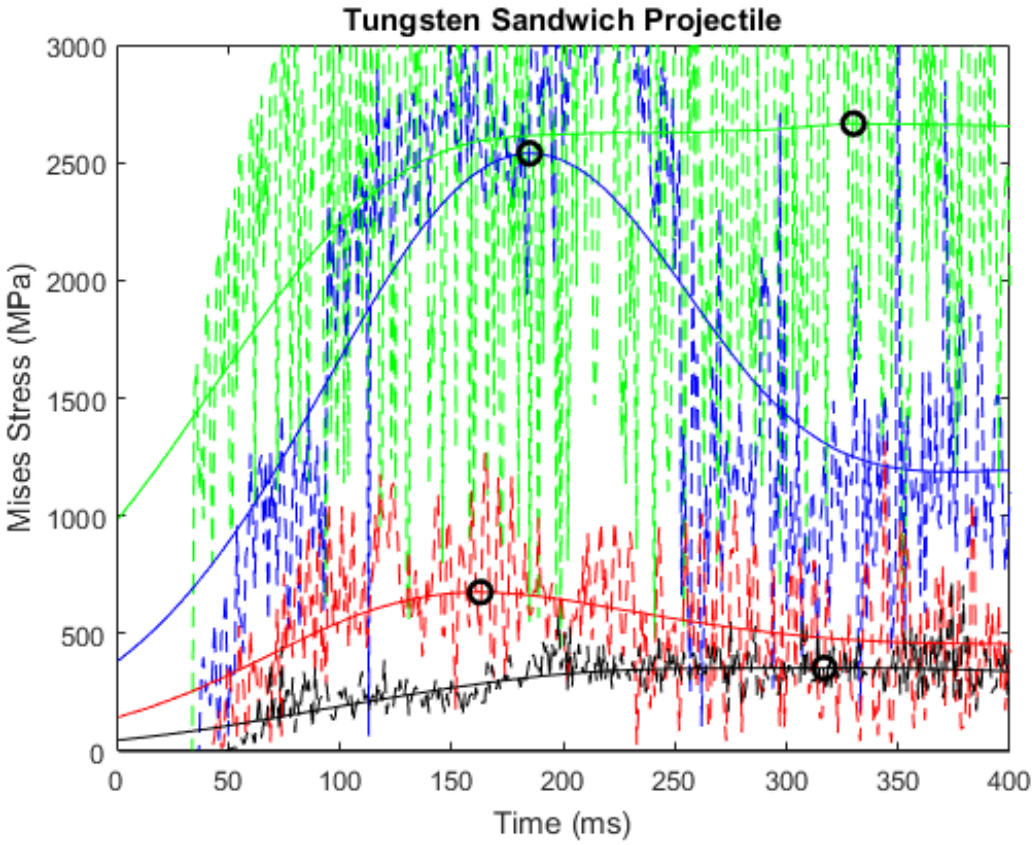

Figure 65. Raw and Smoothed Data for CILA Traced Elements.

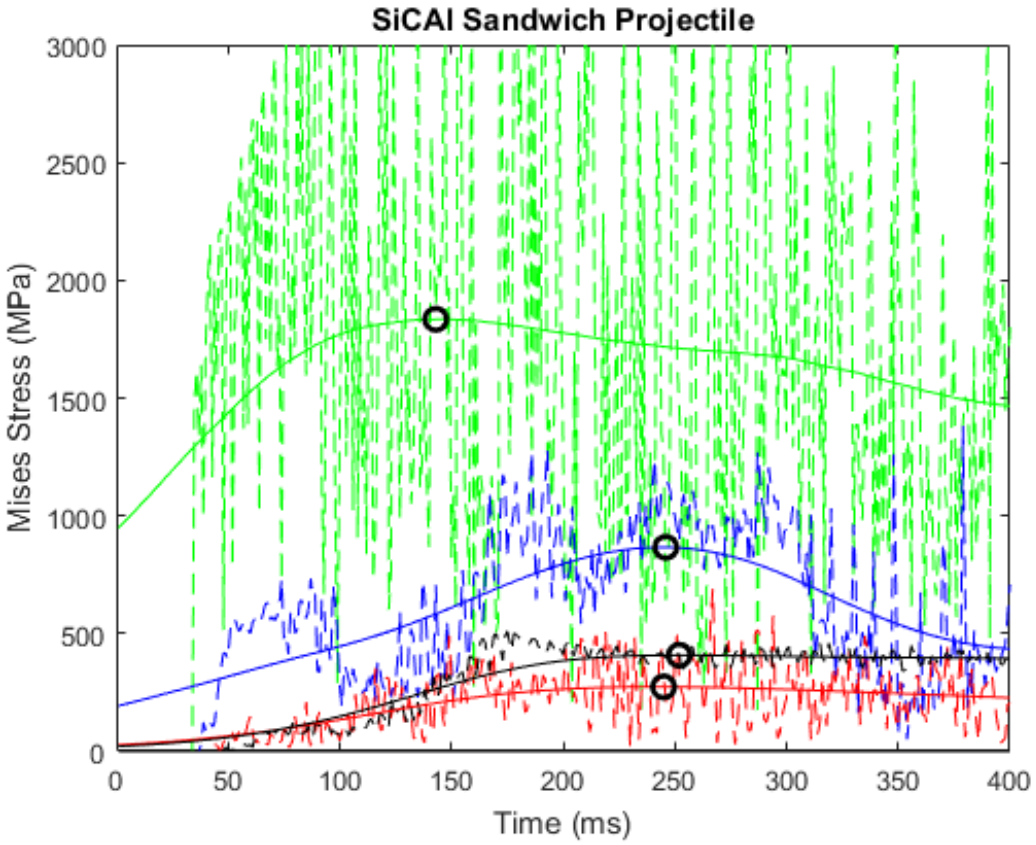

Figure 66. Raw and Smoothed Data for DILA Traced Elements.

Bibliography

1. Driscoll, J. J. and Manucy, A., "Artillery Through the Ages." *Military Affairs*, 1949.

2. Tudor, P. E.-h., "United States Patent (19) BYS4 % C," , No. 19, 1977.

3. Jan, P., " UNITED .sTAT-Es PATENT -," Vol. 12, No. 19, 1943, pp. 2–4.

4. States, U., "Patent Application Publication (10) Pub . No .: US 2006 / 0165926A," Vol. 1, No. 19, 2006, pp. 10–15.

5. Patel, A. A. and Palazotto, A. N., "Investigation of hybrid material projectile impact against concrete targets," *AIAA/ASCE/AHS/ASC Structures, Structural Dynamics, and Materials Conference*, 2018.

6. Richards, H. K. and Liu, D., "Topology optimization of additively-manufactured, lattice-reinforced penetrative warheads," *56th AIAA/ASCE/AHS/ASC Structures, Structural Dynamics, and Materials Conference*, 2015.

7. Graves, W. T., Liu, D., and Palazotto, A. N., "Topology optimization of a penetrating warhead," *Additive Manufacturing Handbook: Product Development for the Defense Industry*, 2017.

8. Provchy, Z. A., Palazotto, A. N., and Flater, P., "Additively manufactured perforators," *58th AIAA/ASCE/AHS/ASC Structures, Structural Dynamics, and Materials Conference, 2017*, 2017.

9. Palazotto, A. N., "Investigation of Blunt and Ogive-nose Projectiles Impact Against Aluminum and Concrete Targets," , pp. 1–9.

10. Huebner, K. H., *The Finite Element Method for Engineers*, Wiley, 2001.

11. Koutromanos, I., *Fundamentals of Finite Element Analysis*, Wiley, 2018.

12. Karami, M. B., Cerit, A. A., and Nair, F., "Surface characteristics of projectiles after frictional interaction with metal matrix composites under ballistic condition," *Wear*, 2006.

13. Laursen, T., *Computational Contact and Impact Mechanics*, Springer, 2002.

14. Hillerborg, A., "Analysis of crack formation and crack growth in concrete by means of fracture mechanics and finite elements," *Cement and Concrete Research*, 1976.

15. Teng, T. L., Chu, Y. A., Chang, F. A., and Chin, H. S., "Simulation model of impact on reinforced concrete," *Cement and Research*, 2004.

16. Jankowiak, T., "Identification of parameters of concrete damage plasticity constitutive model," *Researchgate.Net*, , No. June 2013, 2014.

17. Voyiadjis, G. Z., Al-Rub, R. K., and Palazotto, A. N., "Constitutive modeling and simulation of perforation of targets by projectiles," *AIAA Journal*, 2008.

18. Backman, M. E. and Goldsmith, W., "The mechanics of penetration of projectiles into targets," *International Journal of Engineering Science*, Vol. 16, No. 1, 1978, pp. 1–99.

19. Martin, O., *Comparison of different Constitutive Models for Concrete in ABAQUS / Explicit for Missile Impact Analyses*, 2010.

20. V.Chaudhari, S. and A. Chakrabarti, M., "Modeling of Concrete for Nonlinear Analysis using Finite Element Code ABAQUS," *International Journal of Computer Applications*, 2012.

21. Tyau, J. S., *Finite Element Modeling of Reinforced Concrete Using 3-Dimensional Solid Elements With Discrete Rebar*, Ph.D. thesis, Brigham Young University, 2009.

22. Rosso, M., "Ceramic and metal matrix composites: Routes and properties," 2006.

23. Yen, C.-F., "7 th International LS-DYNA Users Conference Penetration/Explosive BALLISTIC IMPACT MODELING OF COMPOSITE MATERIALS," , pp. 15–26.

24. Bandaru, A. K. and Ahmad, S., "Modeling of progressive damage for composites under ballistic impact," 2016.

25. Murugesan, M. and Jung, D. W., "Johnson cook material and failure model parameters estimation of AISI-1045 medium carbon steel for metal forming applications," *Materials*, 2019.

26. Moxnes, J. F., Teland, J. A., Skriudalen, S., Bergsrud, S. M., Sundem-Eriksen, L., and Fykse, H., *Development of material models for semi-brittle materials like tungsten carbide*, No. November, 2010.

27. Daniel, I. M. and Ishai, O., *Engineering Mechanics of Composite Materials*, Oxford University Press, New York, NY, 2006.

28. Palazatto, A. N., Run, R., and Watt, G., "INTRODUCTION TO METAL MATRIX COMPOSITES IN AEROSPACE APPLICATIONS By Anthony N. Palazotto, 1 Fellow, ASCE, Robert Run, 2 and George Watt 3," *Aerospace*, Vol. 1, No. 1, 1988, pp. 3–17.

29. Barbero, E. J., "Introduction to Composite Materials Design," *CRC Press*, 2011.

30. Al-Ketan, O., Rowshan, R., Palazotto, A. N., and Abu Al-Rub, R. K., "On Mechanical Properties of Cellular Steel Solids with Shell-Like Periodic Architectures Fabricated by Selective Laser Sintering," *Journal of Engineering Materials and Technology, Transactions of the ASME*, Vol. 141, No. 2, 2019, pp. 1–12.

31. Ipson, R. F. R. and W., T., "Ballistic Perforation Dynamics," *Journal of Applied Mechanics*, Vol. 30, No. 3, 1963, pp. 384–391.

32. Newell, D. J., O'Hara, R. P., Cobb, G. R., Palazotto, A. N., Kirka, M. M., Burggraf, L. W., and Hess, J. A., "Mitigation of scan strategy effects and material anisotropy through supersolvus annealing in LPBF IN718," *Materials Science and Engineering A*, 2019.

Vita

Andrew Beard grew up in Appleton, Wisconsin and graduated from Appleton North High School in 2009. He went on to receive his undergraduate degree with a B.S. in Mechanical Engineering from the University of St. Thomas in St. Paul, Minnesota in 2014. Andrew commissioned as a second lieutenant in the United States Air Force shortly after graduating in 2014, and he began his first active duty assignment in 2015 as an Aircrew Flight Equipment Acquisition Engineer for the Human Systems Division, Agile Combat Support Directorate, Air Force Life Cycle Management Center at Wright-Patterson Air Force Base in Dayton, Ohio. In 2017 he became the Executive Officer for the Engineering Directorate, Air Force Life Cycle Management Center at Wright-Patterson Air Force Base in Dayton, Ohio.

Andrew began his assignment at the Air Force Institute of Technology in 2018 and upon graduating will have received a Master's Degree in Aeronautical Engineering.

REPORT DOCUMENTATION PAGE

Form Approved
OMB No. 0704–0188

1. REPORT DATE *(DD–MM–YYYY)*	2. REPORT TYPE	3. DATES COVERED *(From — To)*
26-03-2020	Master's Thesis	Sept 2018 — Mar 2020

4. TITLE AND SUBTITLE

ALTERNATIVE MATERIAL FOR HIGH-SPEED PROJECTILE CASING

5a. CONTRACT NUMBER

5b. GRANT NUMBER

5c. PROGRAM ELEMENT NUMBER

6. AUTHOR(S)

Andrew W. Beard

5d. PROJECT NUMBER

5e. TASK NUMBER

5f. WORK UNIT NUMBER

7. PERFORMING ORGANIZATION NAME(S) AND ADDRESS(ES)

Air Force Institute of Technology
Graduate School of Engineering and Management (AFIT/EN)
2950 Hobson Way
WPAFB OH 45433-7765

8. PERFORMING ORGANIZATION REPORT NUMBER

AFIT/ENY/MS/20/M/255

9. SPONSORING / MONITORING AGENCY NAME(S) AND ADDRESS(ES)

Air Force Office of Scientific Research
875 N. Randolph, Ste.325
Arlington Virginia, 22203
COMM 703-696-7797
Email: info@us.af.mil

10. SPONSOR/MONITOR'S ACRONYM(S)

AFOSR

11. SPONSOR/MONITOR'S REPORT NUMBER(S)

12. DISTRIBUTION / AVAILABILITY STATEMENT

DISTRIBUTION STATEMENT A:
APPROVED FOR PUBLIC RELEASE; DISTRIBUTION UNLIMITED.

13. SUPPLEMENTARY NOTES

14. ABSTRACT

A high-speed projectile impact is a highly complex dynamic problem that can be simplified with the use of finite element analysis solvers. Abaqus/Explicit was used to evaluate the impact of various projectiles using a plane strain setup. Using a baseline stainless steel projectile, the proposed sandwich construction design was analyzed for competition with the baseline. The overall goal was to explore the use of a new casing design and if it could perform similarly to the baseline projectile. The sandwich construction used stainless steel, tungsten, and silicon-carbide reinforced aluminum as outer and inner shell materials. The core material was created using additive manufacturing of inconel 718. The inconel 718 core used a triply periodic minimal surface structure manufactured to provide the projectile casing with high stiffness and strength while reducing the volume of material used to manufacture it. A monolithic concrete target using a brittle cracking model for a projectile hitting a concrete wall in order to simulate a projectile impacting a bunker, road, or other concrete structure.

15. SUBJECT TERMS

Projectile, Abaqus, Explicit, MMC

16. SECURITY CLASSIFICATION OF:			17. LIMITATION OF ABSTRACT	18. NUMBER OF PAGES	19a. NAME OF RESPONSIBLE PERSON
a. REPORT	b. ABSTRACT	c. THIS PAGE			Dr. Anthony Palazotto, AFIT/ENY
U	U	U	UU	88	19b. TELEPHONE NUMBER *(include area code)* (937) 255-3636, x4599; anthony.palazotto@afit.edu